

FlashSVD: Memory-Efficient Inference with Streaming for Low-Rank Models

Zishan Shao^{1,2*}, Yixiao Wang², Qinsi Wang², Ting Jiang², Zhixu Du², Hancheng Ye², Danyang Zhuo³, Yiran Chen², Hai Li²

¹Department of Statistical Science

²Department of Electrical & Computer Engineering

³Department of Computer Science

Abstract

Singular Value Decomposition (SVD) has recently seen a surge of interest as a simple yet powerful tool for large language models (LLMs) compression, with a growing number of works demonstrating 20-80% parameter reductions at minimal accuracy loss. Previous SVD-based approaches have focused primarily on reducing the memory footprint of model weights, largely overlooking the additional activation memory overhead incurred during inference when applying truncated factors via standard dense CUDA kernels. Our experiments demonstrate that this activation overhead, scaling with sequence length and hidden dimension, prevents current SVD compression techniques from achieving any reduction in peak inference memory, thereby limiting their viability for real-world, on-device deployments.

We introduce **FlashSVD**, a novel, end-to-end rank-aware streaming inference framework specifically designed for SVD-compressed large language models. FlashSVD can be seamlessly integrated with any model that employs SVD-based methods for parameter reduction. By fusing low-rank projection kernels directly into both the self-attention and feed-forward network (FFN) pipelines, FlashSVD avoid materializing full-size activation buffers. Instead, small tiles of the truncated factors are loaded into on-chip SRAM, multiplied and reduced on the fly, and immediately evicted, preserving high GPU occupancy and adding no extra latency. On standard encoder benchmarks (e.g., BERT-Base), FlashSVD cuts peak activation memory by up to 70.2% and intermediate transient memory by 75%, all while incur no accuracy loss with upstreaming compression methods, offering a practical path toward memory-constrained deployment of low-rank LLMs.

1. Introduction

Recent advances in Transformer architectures have yielded state-of-the-art performance across diverse tasks with the cost of ever-increasing model size and computational complexity. Rapid scaling of model size poses non-negligible challenges on deploying large pre-trained models on edge devices due to stringent *peak memory* constraints: activations and full-precision weights together often exceed available high-bandwidth memory (HBM), leading to out-of-memory (OOM) failures even for moderately sized context. While parameter compression techniques such as truncated singular value decomposition (SVD) can reduce model size by over 50% with minimal accuracy loss [10, 30], they do not address the *activation* memory spikes during inference. In practice, mainstream inference backends (e.g., FlashAttention [2, 3], xFormers [31], Megatron [23]) offer no

*Correspondence E-mail: zishan.shao@duke.edu

native support for low-rank layers, so peak memory remains dominated by large intermediate buffers, almost as high as in fully dense implementations when using these inference backends.

Concurrent with advances in model compression, extensive research has targeted activation-aware optimizations for dense transformers. Key-value caching in autoregressive decoders reuses past attention states to eliminate redundant $O(BM^2)$, where B is the batch size and M is the sequence length, computations and storage overhead [20]. FlashAttention further accelerates both training and inference by fusing the softmax and matrix-multiply operations into a single GPU kernel, thereby obviating the need to materialize full attention score matrices [2, 3]. Complementary methods such as mixed-precision arithmetic, quantization, and structured pruning have also proven effective at reducing compute and memory demands without modifying the core transformer architecture [4, 8, 12, 29, 9, 13, 18, 19, 15, 7]. Despite these infrastructural and algorithmic innovations for dense and block-sparse layers, prior SVD-based compression techniques focus on dense model weights factorization but still execute inference with standard dense matrix kernels—thereby overlooking both activation memory overhead and the opportunity to tailor computations to low-rank structure.

In this work we introduce **FlashSVD**, an end-to-end inference framework that enables rank-aware activation for SVD-based low-rank models. Our key contributions are:

- We identify that activation memory—alongside fixed parameter cost—dominates inference overhead, whereas prior work has largely targeted weight compression. We propose rank-aware fine-tuning as a promising direction to drive ranks lower without sacrificing accuracy, yielding further activation-cost reductions.
- We proposed two series of rank-aware streaming low-rank kernels that consumes only low-rank activations in a single pass with no memory-expensive dense intermediates while ensure computational efficiency in moderate-large context window (Theorem 2, 4, 9, 10).
- By exploiting the multi-head structure when compressing the attention projection matrices, the necessary rank-loss ratio $1 - \frac{r_{\text{retained}}}{r_{\max}}$ is substantially lower than that required by single-head compression methods in prior works, thereby permitting more moderate rank reductions while still achieving comparable overall compression performance.

2. Related Work

Low-Rank Weight Compression SVD-based factorization is a classical approach for transformer compression, where small singular values are truncated under the Eckart–Young–Mirsky theorem to reduce parameter counts at some cost of accuracy [30, 27]. Activation-aware SVD (ASVD) introduces rank awareness into both weight and KV-cache compression for decoders, factorizing cache states into low-rank components to achieve up to 30 % weight reduction and 50 % KV-cache memory savings with no retraining [30]. Building on this idea, SVD-LLM (v1-v2) [27, 28] also stores KV-cache in low-rank form but further employs a lightweight calibration set to determine optimal truncation thresholds, thereby preserving downstream performance despite more aggressive compression. MoDeGPT partitions each Transformer block into modular subcomponents and applies Nyström, CR decomposition, and SVD at the module level – enabling structured, fine-tuning-free compression that saves up to 30% compute and increases inference throughput by 46% on 13B models [14]. Dobi-SVD makes the truncation process differentiable by learning per-layer cut positions via gradient-based optimization and deriving optimal low-rank updates, thus maintaining performance under 40% parameter compression [26]. Palu [1] introduced a rank-aware KV-Cache compression scheme that dynamically adapts the low-rank approximation of cached keys and values per attention head that significantly reducing memory footprint without degrading retrieval accuracy for the SVD decomposed models.

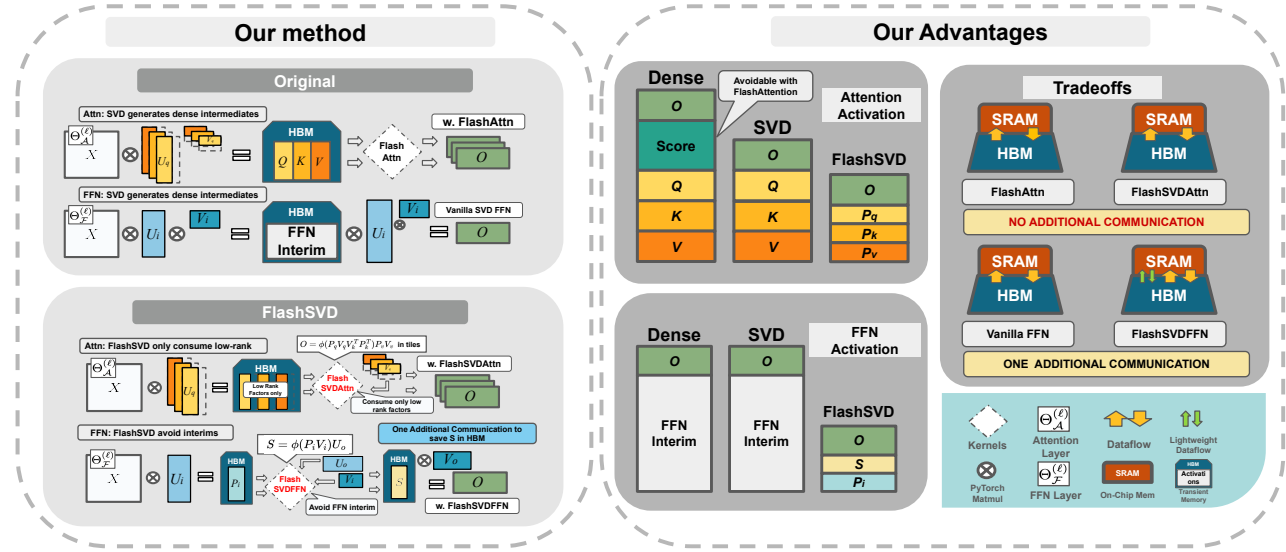


Fig. 1: FlashSVD fuses low-rank projections into both the self-attention and FFN stages by streaming small tiles of the truncated U and V factors through on-chip SRAM instead of materializing dense activation matrices in HBM. **FlashSVDAttn** only consumes low-rank factors, reducing complexity from $O(BMD_{\mathcal{A}}^{\Theta})$ to $O(BMr_{\Theta^*})$. In the FFN, inputs are first projected into the low-rank factor space via a cuBLAS GEMM (for standard matrix multiplication) and then passed through **FlashSVDFNN** in one pass, avoiding any $O(BMD_{\mathcal{F}}^{\Theta})$ intermediate activations and ensuring the rank-aware HBM performance.

Streaming Inference FlashAttention reorders the standard attention computation into tiled matrix-multiply and softmax steps that fit in on-chip SRAM, thereby minimizing HBM-SRAM transfers and achieving up to 3 \times end-to-end speedups on GPT-2 with exact numerical equivalence to dense attention [2]. FlashAttention-2 and -3 optimize work partitioning and kernel fusion to sustain 50–73 % of peak FLOPs on NVIDIA A100s, and FlashAttention-3 on H100s delivers 1.5–2.0 \times speedups in FP16 (up to 740 TFLOPs/s, 75 % utilization) and near 1.2 PFLOPs/s in FP8—with 2.6 \times lower numerical error than baseline FP8 attention [3, 21]. BlockLLM introduces a block-parallel inference engine that shards and caches KV blocks across multiple concurrent workflows, reducing redundant memory loads and lowering per-token latency by as much as 33% in multi-tenant serving scenarios [22]. Star Attention partitions long-sequence inputs across hosts in two phases—a block-local intra-node attention followed by a global inter-node aggregation—enabling exact, distributed attention on sequences exceeding 64K tokens with sublinear communication overhead [16].

Fine-Tuning & Hybrid Compression LoRA inserts trainable, low-rank adaptation matrices into the frozen weights of each Transformer layer, reducing the number of fine-tuned parameters by over four orders of magnitude while matching full-fine-tuning performance on tasks such as GLUE and SQuAD [11]. QLoRA builds on this by first quantizing all model weights to 4-bit integers using NormalFloat and GPTQ techniques, then applying LoRA to the quantized weights; this combination enables fine-tuning of 65B-parameter LLMs on a single 48 GB GPU with negligible quality loss [4].

Although low-rank SVD compressors and I/O-aware streaming kernels have each shown dramatic gains, they have developed in isolation: SVD methods focus on offline factorization with no regard for GPU memory-I/O or block-parallel execution, while streaming kernels target dense weights. There is limited work in developing a rank-aware streaming kernels for SVD-based low-rank models inference. We bridge this gap with two families of rank-aware GPU kernels that eliminate memory-intensive dense activation materialization. Our method is

agnostic to the upstream SVD compression – applicable to any SVD-compressed model without degrading accuracy.

3. Methodology

Optimal Low-Rank Factorization via SVD Let $W \in \mathbb{R}^{m \times n}$ be a dense matrix (e.g. a full self-attention projection matrix). Its full singular value decomposition

$$W = U \Sigma V^\top, \Sigma = \text{diag}(\sigma_1, \dots, \sigma_{\min\{m,n\}}), \quad (1)$$

$$\sigma_i \geq \sigma_j, \quad \forall i > j.$$

yields the best rank- r approximation in Frobenius norm by the Eckart–Young–Mirsky theorem [6]. Concretely, truncating to the top- r singular values gives

$$W^{[r]} = U_{[:,1:r]} \Sigma_{[1:r,1:r]} V_{[:,1:r]}^\top,$$

which provably minimizes $\|W - W^{[r]}\|_F$ over all rank- r matrices. For simplicity, we evenly distribute the singular values, rewriting as $W^{[r]} = \tilde{U} \tilde{V}^\top$ where $\tilde{U} = U_{[:,1:r]} \Sigma^{1/2}$ and $\tilde{V} = V_{[:,1:r]} \Sigma^{1/2}$.

Model Decomposition For a general large-language model $\Theta = \{\Theta_{\mathcal{A}}^{(\ell)} \cup \Theta_{\mathcal{F}}^{(\ell)}\}_{\ell=1}^L$, where $\Theta_{\mathcal{A}}^{(\ell)}$ and $\Theta_{\mathcal{F}}^{(\ell)}$ denote the attention and FFN parameters in block ℓ . Equivalently, grouping across layers gives $\Theta = \{\Theta_{\mathcal{A}}^{(\ell)}\}_{\ell=1}^L \cup \{\Theta_{\mathcal{F}}^{(\ell)}\}_{\ell=1}^L$, so truncated SVD can be independently applied layer-wise on each $\Theta_{\mathcal{A}}^{(\ell)}$ and $\Theta_{\mathcal{F}}^{(\ell)}$ subfactors, enabling fine-grained, per-layer rank selection and compression. We apply rank- r_{Θ^*} truncated SVD (Definition 1, 2) to each dense projection matrix in a Transformer block, where the rank for the self-attention module follows Theorem 3, while the FFN rank is selected according to Theorem 5. The resulting compressed model is denoted Θ^* , so that $r_{\Theta^*} = r_{\Theta^*}$. These rank choices directly influence the memory–compute trade-offs described in Theorem 14. The self-attention projections are square matrices of size $\mathcal{D}_{\mathcal{A}}^\Theta$, while the FFN projection matrices W_i^\top and W_o are rectangular of shape $\mathcal{D}_{\mathcal{F}}^\Theta \times \mathcal{D}_{\mathcal{A}}^\Theta$.

Streaming Activations In standard multi-head self-attention calculation, one forms the full score matrix $\text{Softmax}\left(\frac{QK^\top}{\sqrt{d_{\Theta_{\mathcal{A}},h}}}\right) \in \mathbb{R}^{B \times M \times M}$, where $d_{\Theta_{\mathcal{A}},h} = \mathcal{D}_{\mathcal{A}}^\Theta / H$, $\forall h \in \{1, \dots, H\}$, B is batch size, and M is sequence length, incurring $\mathcal{O}(BM^2)$ off-chip memory and bandwidth per head. FlashAttention [2, 3] instead tiles and streams the queries, keys, and values, small blocks of Q , K and V , sized to fit the GPU’s shared memory per streaming multiprocessor, are loaded on-chip, dot-products are then computed and softmaxed with streaming, and results are immediately accumulated in full FP32 precision without ever materializing the full $B \times H \times M^2$ matrix on HBM. Consequently, HBM memory complexity for attention computation drops from $\mathcal{O}(BHM^2)$ to $\mathcal{O}(BH M d_{\Theta_{\mathcal{A}},h})$ for H heads attention, enabling state-of-the-art attention computation performance in both training and inference.

FlashSVDAttention FlashSVDAttention (Theorem 2) enable rank-aware streaming by consuming only the low-rank factors of each head’s query, key, and value projections:

$$P_q, P_k, P_v \in \mathbb{R}^{B \times M \times r_{\Theta^*}}, \quad V_q, V_k, V_v \in \mathbb{R}^{r_{\Theta^*} \times d_{\Theta_{\mathcal{A}},h}}.$$

Algorithm 1 FlashSVDAttention Forward Pass

```

1: PART I. SUBROUTINE LOAD_TILES:
2: Input: Factor  $P_a \in \mathbb{R}^{B \times B_M \times r_{\Theta^*}}$ , projection  $V_a \in \mathbb{R}^{r_{\Theta^*} \times d_{\Theta_{\mathcal{A}},h}}$ , bias  $b_a \in \mathbb{R}^{d_{\Theta_{\mathcal{A}},h}}$ , tile size  $B_R$ , rank  $r_{\Theta^*}$ , padded rank  $R = \lceil \frac{r_{\Theta^*}}{B_R} \rceil \cdot B_R$ 
3: Output: Reconstructed tiles  $A_{\text{tile}}$  for each  $r$  with padding mask
4: for  $r = 0$  to  $R$  step  $B_R$  do
5:    $A_{\text{tile}} \leftarrow P_a[:, :, r : r + B_R] V_a[r : r + B_R, :] + b_a$ 
6: end for
7: PART II. FLASHSVDATTENTION FORWARD PASS:
8: Input: Low-rank factors  $P_q, P_k, P_v \in \mathbb{R}^{B \times M \times r_{\Theta^*}}$ , projections  $V_q, V_k, V_v \in \mathbb{R}^{r_{\Theta^*} \times d_{\Theta_{\mathcal{A}},h}}$ , biases  $b_q, b_k, b_v \in \mathbb{R}^{d_{\Theta_{\mathcal{A}},h}}$ , tile size  $B_M$  and  $B_R$ , sequence length  $M$ 
9: Output: Output  $O \in \mathbb{R}^{B \times M \times d_{\Theta_{\mathcal{A}},h}}$ 
10: Initialize  $O \leftarrow 0$ 
11: for  $\ell = 0$  to  $M - 1$  step  $B_M$  do
12:   Reconstruct  $Q$  block on-chip
13:    $Q_{\text{tile}} \leftarrow \text{LOAD\_TILES}(P_q[:, \ell : \ell + B_M, :], V_q[:, :, \ell : \ell + B_M], b_q, B_R)$ 
14:   for  $m = 0$  to  $M - 1$  step  $B_M$  do
15:     Reconstruct  $K$  and  $V$  blocks on-chip
16:      $K_{\text{tile}} \leftarrow \text{LOAD\_TILES}(P_k[:, \ell : \ell + B_M, :], V_k[:, :, \ell : \ell + B_M], b_k, B_R)$ 
17:      $V_{\text{tile}} \leftarrow \text{LOAD\_TILES}(P_v[:, \ell : \ell + B_M, :], V_v[:, :, \ell : \ell + B_M], b_v, B_R)$ 
18:     Compute attention scores and softmax
19:      $\text{scores} \leftarrow Q_{\text{tile}} (K_{\text{tile}})^T / \sqrt{d_{\Theta_{\mathcal{A}},h}}$ 
20:      $\alpha \leftarrow \text{STREAM-SOFTMAX}(\text{scores}, \text{axis} = -1)$ 
21:     [2]
22:      $O[:, \ell : \ell + B_M, :] += \alpha V_{\text{tile}}$ 
23:   end for
24: end for

```

where the P_a factors are formulated from XU_a , and $V_a \forall a \in \{q, k, v\}$. Internally the kernel tiles the $(M, d_{\Theta_{\mathcal{A}},h})$ plane into small $(B_M, d_{\Theta_{\mathcal{A}},h})$ blocks that stream through on-chip SRAM. For each tile it (1) forms the local low-rank query block $Q_{\text{tile}} = P_{q,\text{tile}} V_{q,\text{tile}} + b_q$ with iterative accumulation over r_{Θ^*} , (2) multiplies and accumulates score with corresponding reconstructed key blocks $K_{\text{tile}} = P_{k,\text{tile}} V_{k,\text{tile}} + b_k$, (3) applies a row-wise softmax, and (4) weights and reduces the value factors $P_{v,\text{tile}} V_{v,\text{tile}}$ to produce the output slice. By fusing the two small GEMMs and the softmax into one pass, and never materializing the full $B \times H \times M \times d_{\Theta_{\mathcal{A}},h}$ score or output buffers off-chip, FlashSVDAttn attains the rank-aware $O(Hr_{\Theta^*}(B M + d_{\Theta_{\mathcal{A}},h}))$ HBM bound proven in Theorem 4.

FlashSVDFFN Once the FlashAttention alleviated the peak-memory burden of self-attention [2, 3], the feed-forward network (FFN) becomes the new dominant factor (theorem 8). Even when W_i and W_o admit low-rank decompositions $W_i^{[r_{\Theta^*}]} = U_i V_i$ and $W_o^{[r_{\Theta^*}]} = U_o V_o$ with ranks $r_{\Theta^*} \ll D_{\mathcal{F}}^{\Theta}$, the intermediate $\phi(XU_i V_i + b_i) \in \mathbb{R}^{(B \times M) \times D_{\mathcal{F}}^{\Theta}}$ must still be materialized in full, dominating HBM despite in low-rank case (theorem 8). We propose two rank-aware streaming FFN variants to eliminate this large interim activation that trade off compute versus I/O: a mild version that maximizes reuse of vendor-tuned GEMM kernels at the cost of extra off-chip traffic, and an extreme version that enable zero I/O to HBM.

FlashSVDFFN V1 (Rank-Aware Fusion) First, the input is projected into the factor space with $P = XU_i$ via the cuBlas GEMM, storing $(B \times M) \times r_i$ sized intermediate in HBM. Second, a lightweight streamed kernel applies the nonlinearity and the next projection in one fused pass by computing $S = \phi(PV_i + b_i)U_o$ according to algorithm 2 without ever materializing the full $(B \times M) \times D_{\mathcal{F}}^{\Theta}$ activation. Finally, the output is reconstructed

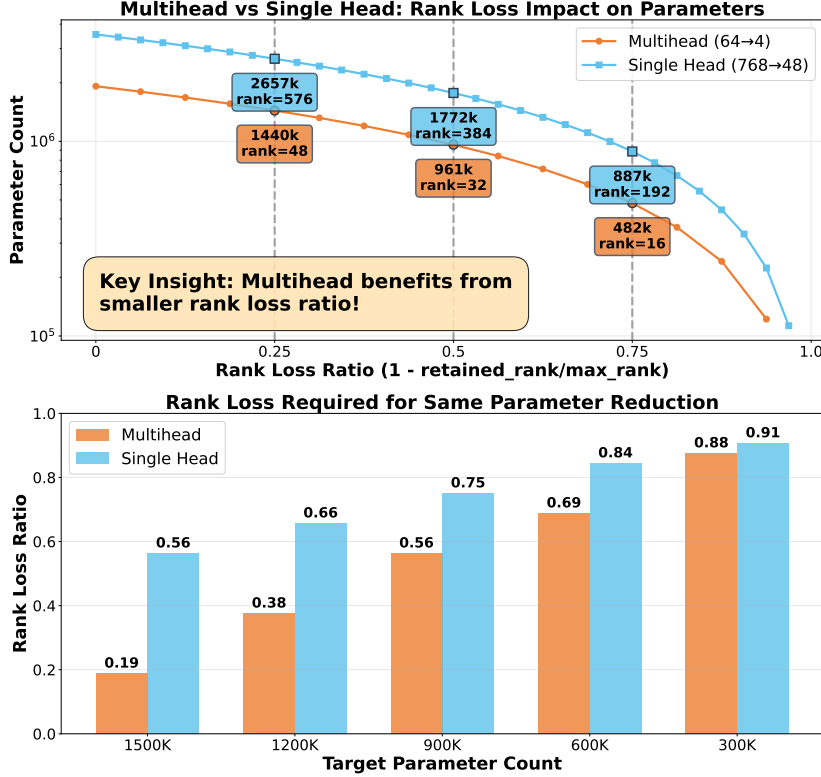


Fig. 2: Multi-head SVD compresses model attention projection matrices more gently than single-head SVD.

with $O = S V_o + b_o$ via a second cuBlas GEMM. Because both P and S remain bounded by the truncated rank r_{Θ^*} , the overall computation and intermediate memory scale with r_{Θ^*} with the tradeoff for two extra I/O with HBM, directly yielding the tight bounds on activation memory and FLOP reduction stated in Theorem 9 and Theorem 14.

FlashSVDFFN V2 (Extreme-Case) employs a single fused GEMM–Activation–GEMM GPU kernel to stream the low-rank FFN forward pass by directly loading X , projection factors U_i, V_i, U_o, V_o , and biases b_i, b_o on-the-fly, incurring no additional arithmetic cost or asymptotic complexity compared to a dense FFN (identical $O(B M r_{\Theta^*} D_{\mathcal{F}}^{\Theta} + B M r_{\Theta^*} D_{\mathcal{A}}^{\Theta})$ FLOPs). This unified pipeline supports arbitrary activations $\phi(\cdot)$, and theoretically pushes the lower bound for variable part of rank-aware activation compression to zero (see Theorem 10). By launching one kernel block per tile and accumulating directly into the output buffer, we avoid any materialized $(B \times M) \times \mathcal{D}_{\mathcal{F}}^{\Theta}$ mid-buffers, achieving the $O(r_{\Theta^*}(B M + \mathcal{D}_{\mathcal{F}}^{\Theta}))$ HBM bound of Theorem 9.

Multi-Head Attention Amplifies SVD Savings Many recent compression schemes (e.g., ASVD [30], Dobi-SVD [26]) apply SVD to the entire $\mathcal{D}_{\mathcal{A}}^{\Theta} \times \mathcal{D}_{\mathcal{A}}^{\Theta}$ attention projection as a single matrix. This single head approach only yields parameter reduction when $r_{\Theta^*} < \frac{1}{2} \mathcal{D}_{\mathcal{A}}^{\Theta}$, and in practice forces drastic rank cuts that frequently degrade accuracy and limits the overall compression capacity of SVD-based method. In contrast, the native multi-head structure splits $\mathcal{D}_{\mathcal{A}}^{\Theta}$ into H heads of size $d_{\Theta, h} = \mathcal{D}_{\mathcal{A}}^{\Theta}/H$. By applying truncated SVD per head, the threshold for parameter compression drops to $r_{\Theta^*} < \frac{\mathcal{D}_{\mathcal{A}}^{\Theta}}{H+1}$. As Figure 2 illustrates, compressing BERT’s head projections to 1.5 M parameters requires a 56% rank reduction under single-head SVD, risking severe quality

Algorithm 2 FlashSVDFFN Forward Pass V1

Require: Input $X \in \mathbb{R}^{B \times M \times \mathcal{D}_{\mathcal{A}}^{\Theta}}$; SVD factors $U_i \in \mathbb{R}^{\mathcal{D}_{\mathcal{A}}^{\Theta} \times r_{\Theta^*}}$, $V_i \in \mathbb{R}^{r_{\Theta^*} \times \mathcal{D}_{\mathcal{F}}^{\Theta}}$, $b_i \in \mathbb{R}^{\mathcal{D}_{\mathcal{F}}^{\Theta}}$;
 $U_o \in \mathbb{R}^{\mathcal{D}_{\mathcal{F}}^{\Theta} \times r_{\Theta^*}}$, $V_o \in \mathbb{R}^{r_{\Theta^*} \times \mathcal{D}_{\mathcal{A}}^{\Theta}}$, $b_o \in \mathbb{R}^{\mathcal{D}_{\mathcal{A}}^{\Theta}}$; number of blocks G ; nonlinearity $\phi(\cdot)$.

Ensure: $O \in \mathbb{R}^{B \times M \times \mathcal{D}_{\mathcal{A}}^{\Theta}}$

- 1: $B_M \leftarrow \lceil M/G \rceil$, $B_{D_{\mathcal{F}}^{\Theta}} \leftarrow \lceil \mathcal{D}_{\mathcal{F}}^{\Theta}/G \rceil$
- 2: GEMM 1st: project into factor-space (cuBlas)
- 3: $P \leftarrow X U_i \{(BM) \times r_{\Theta^*}\}$
- 4: On-Chip: rank-aware activation streaming
- 5: **for** $\ell = 0$ to $M - 1$ **step** B_M **do**
- 6: initialize $Z_{\text{tile}} \leftarrow 0_{B \times B_M \times r_{\Theta^*}}$
- 7: **for** $d = 0$ to $\mathcal{D}_{\mathcal{F}}^{\Theta} - 1$ **step** $B_{D_{\mathcal{F}}^{\Theta}}$ **do**
- 8: $V_i^{(d)} \leftarrow V_i[:, d : d + B_{D_{\mathcal{F}}^{\Theta}}] \{(r_{\Theta^*} \times B_{D_{\mathcal{F}}^{\Theta}})\}$
- 9: $U_o^{(d)} \leftarrow U_o[d : d + B_{D_{\mathcal{F}}^{\Theta}}, :] \{(B_{D_{\mathcal{F}}^{\Theta}} \times r_{\Theta^*})\}$
- 10: $b_i^{(d)} \leftarrow b_i[d : d + B_{D_{\mathcal{F}}^{\Theta}}] \{(B_{D_{\mathcal{F}}^{\Theta}})\}$
- 11: $Y \leftarrow \phi(P V_i^{(d)} + b_i^{(d)}) \{B \times B_M \times B_{D_{\mathcal{F}}^{\Theta}}\}$
- 12: $Z_{\text{tile}} += Y U_o^{(d)} \{(B \times B_M \times B_{D_{\mathcal{F}}^{\Theta}}) \times (B_{D_{\mathcal{F}}^{\Theta}} \times r_{\Theta^*})\}$
- 13: **end for**
- 14: $Z \leftarrow Z_{\text{tile}} \{(BM) \times r_{\Theta^*}\}$
- 15: **end for**
- 16: GEMM 2nd: project to model-space (cuBlas)
- 17: $O \leftarrow Z V_o + b_o \{(BM) \times \mathcal{D}_{\mathcal{A}}^{\Theta}\}$

loss, whereas multi-head SVD needs only a 19% cut, achieving the same compression with far gentler rank pruning.

4. Analysis

FlashSVD establishes provable memory efficient upper bounds on dominant activations during inference by exploiting low-rank structure. Below, we summarize the key theorems that characterize these activation bounds and clarify the fundamental time–memory trade-offs in FlashSVD.

Peak Memory Footprint Analysis Table 1 demonstrates that combining *FlashSVDAttention* with *FlashSVDFFN* reduces the activation memory footprint from $\mathcal{O}(BM(\mathcal{D}_{\mathcal{F}}^{\Theta} + \mathcal{D}_{\mathcal{A}}^{\Theta} + M))$ to $\mathcal{O}(r_{\Theta^*}(BM + \mathcal{D}_{\mathcal{F}}^{\Theta} + \mathcal{D}_{\mathcal{A}}^{\Theta}))$. The FFN memory can be further reduced using *FlashSVDFFN-V2*, and ultimately brought variable part to zero. In the typical regime where $r_{\Theta^*} \ll \mathcal{D}_{\mathcal{A}}^{\Theta}$, $\mathcal{D}_{\mathcal{F}}^{\Theta}$, BM , these optimizations yield a ranked-bounded reduction in HBM activation.

Rank Sensitivity The memory footprint of FlashSVD depends critically on the selected SVD rank r_{Θ^*} . For the attention module, lowering the rank by one in a single head saves $\Delta\mathcal{M}_{\text{flash-svd-attn-single}} = \mathcal{O}(BM + \mathcal{D}_{\mathcal{A}}^{\Theta})$ words, as proved in Proposition 4. Applied across all H heads, the aggregate saving is $\Delta\mathcal{M}_{\text{flash-svd-attn-multi}} = \mathcal{O}(H(BM + d_{\Theta_{\mathcal{A}},h}))$ (Proposition 5).

An analogous result holds for the feed-forward network. Proposition 7, 8 shows that a unit decrease in rank reduces off-chip memory by

$$\Delta\mathcal{M}_{\text{flash-svd-ffn}} \leq \mathcal{O}(BM + D_{\mathcal{F}}^{\Theta}),$$

demonstrating that FFN layers benefit from rank reduction along both the batch-sequence and feature dimensions.

Table 1: Peak HBM \mathcal{M} Complexity for each sub-module. See Theorems 2, 4, 9, 10 in Appendix, Supplementary.

Module	$\mathcal{M}_{\text{dense}}$	$\mathcal{M}_{\text{FlashSVD}}$
Single-Head Attn.	$3BM\mathcal{D}_{\mathcal{A}} + BM^2$	$O(r_{\Theta^*}(BM + \mathcal{D}_{\mathcal{A}}))$
Multi-Head Attn.	$BM\mathcal{D}_{\mathcal{A}}$	$O(r_{\Theta^*}(BM + \mathcal{D}_{\mathcal{A}}))$
FFN-V1	$BM\mathcal{D}_{\mathcal{F}}$	$O(r_{\Theta^*}(BM + \mathcal{D}_{\mathcal{F}}))$
FFN-V2	$BM\mathcal{D}_{\mathcal{F}}$	$O(r_{\Theta^*}\mathcal{D}_{\mathcal{F}})$

Speedup and Latency Analysis We analyze the performance benefits of FlashSVD along three dimensions: FLOP count, memory I/O volume, and end-to-end latency.

Theoretical FLOP savings arise from replacing dense matrix multiplications with low-rank projections: the full-rank computation costs $O((D_{\mathcal{A}}^{\Theta})^2 MB + D_{\mathcal{A}}^{\Theta} D_{\mathcal{F}}^{\Theta} MB)$, while the low-rank version requires only $O(r_{\Theta^*}^2 MB + r_{\Theta^*} D_{\mathcal{A}}^{\Theta} MB + r_{\Theta^*} D_{\mathcal{F}}^{\Theta} MB)$. The resulting asymptotic speedup factor is given in Theorem 14:

$$\Theta\left(\frac{(D_{\mathcal{A}}^{\Theta})^2 + D_{\mathcal{A}}^{\Theta} D_{\mathcal{F}}^{\Theta}}{r_{\Theta^*}^2 + r_{\Theta^*} D_{\mathcal{A}}^{\Theta} + r_{\Theta^*} D_{\mathcal{F}}^{\Theta}}\right).$$

In terms of data movement, the full-rank model must load all query/key/value activations and FFN outputs, with total volume $O(BM(D_{\mathcal{A}}^{\Theta} + D_{\mathcal{F}}^{\Theta}))$ as shown in Theorem 15. In contrast, FlashSVD only needs to read and write low-rank components, yielding reduced volume

$$O(MBr_{\Theta^*} + r_{\Theta^*} D_{\mathcal{A}}^{\Theta} + r_{\Theta^*} D_{\mathcal{F}}^{\Theta}),$$

also see Theorem 15.

Finally, following the roofline model, the end-to-end latency per layer is bounded below by the slower of the compute- and bandwidth-limited paths:

$$T \geq \max\left\{\frac{\text{FLOPs}}{\text{PeakFLOP/s}}, \frac{4N_{\text{bytes}}}{\beta}\right\},$$

where $N_{\text{bytes,in}}$ is the number of input bytes and β is the memory bandwidth in bytes/s, as formalized in Theorem 15.

5. Experiment

5.1. Experimental Setup

Model Setup While the prior activation-aware inference methods (e.g., ASVD [30], Palu [1]) have focused primarily on decoder-side KV-Cache compression for causal LMs, the encoder-side activation overhead remains largely unexplored. FlashSVD naturally extends to decoder models, but since KV-Cache overheads are already well-studied, our evaluation concentrates on encoder architectures. Concretely, we target the most widely adopted compressed encoder pipelines, including naive SVD-BERT, fine-tuned low-rank BERT (FWSVD-BERT), and our fully fused FlashSVD-BERT-applied to BERT and RoBERTa. To isolate the impact of our fusion kernels, we perform an ablation study-toggling FlashSVDAttn and FlashSVDFFN (with autotuned streaming block size) independently across diverse settings of inputs. Decoder-side experiments should follow a similar protocol on causal language models, but our primary focus remains the encoder.

Table 2: Main Results: Base Mem (Base), Total Mem (Peak), Transient Mem (Tran), Latency (Lat), Accuracy (Acc), Compression Ratio (Ratio), batch = 64, ratio = 25%, 50%, **All Training-Free**

Methodology	Base	BERT Experiments														
		sst2					qqp					mnli				
		Peak	Tran	Lat	Acc	Ratio	Peak	Tran	Lat	Acc	Ratio	Peak	Tran	Lat		
Dense																
Vanilla SVD	418.7	695.0	277.3	79.7	92.32	1.00	971.1	553.5	147.3	90.93	1.00	1547.4	1129.7	310.2	84.06	1.00
Parameter Ratio: 25%																
Vanilla SVD	332.4	741.6	409.1	161.1	85.16	-	1149.7	817.3	200.2	72.80	-	1990.0	1657.5	359.7	66.73	-
FlashSVD v1	332.4	576.7	244.2	188.8	85.16	0.60	785.8	453.4	264.8	72.82	0.55	1230.2	897.7	490.5	66.71	0.54
FlashSVD v2	332.4	576.7	244.2	253.5	85.16	0.60	785.8	453.4	400.9	72.81	0.55	1230.2	897.7	753.0	66.71	0.54
FWSVD	332.4	913.6	581.1	83.8	89.91	-	1692.7	1360.3	194.0	84.80	-	3853.0	3520.5	463.2	78.01	-
FlashFWSVD	332.4	541.6	209.2	139.6	89.91	0.36	756.8	424.4	269.3	84.78	0.31	1213.2	880.8	479.9	77.90	0.25
Parameter Ratio: 50%																
Vanilla SVD	249.7	653.5	403.8	150.8	66.88	-	1057.1	807.4	180.4	64.05	-	1888.4	1638.7	321.1	37.92	-
FlashSVD v1	249.7	461.6	211.8	141.6	66.88	0.52	673.3	423.5	193.5	64.05	0.52	1120.7	870.9	350.6	37.81	0.53
FlashSVD v2	249.7	461.6	211.8	192.9	66.88	0.52	673.3	423.5	313.2	64.05	0.52	1120.7	870.9	584.7	37.82	0.53
FWSVD	249.7	821.1	571.3	66.5	79.44	-	1592.2	1342.5	165.5	63.75	-	3734.3	3484.5	427.8	51.06	-
FlashFWSVD	249.7	453.4	203.7	101.5	79.44	0.36	665.3	415.6	189.9	63.75	0.31	1112.5	862.8	341.4	50.92	0.25
RoBERTa Experiments																
Dense	475.5	753.0	277.5	78.1	94.17	1.00	1029.1	553.6	110.1	91.3	1.00	1605.4	1129.9	217.5	87.59	1.00
Parameter Ratio: 25%																
Vanilla SVD	390.3	883.4	493.1	119.2	49.20	-	1375.5	985.3	148.6	60.63	-	2383.8	1993.5	225.0	33.37	-
FlashSVD v1	390.3	634.5	244.2	184.0	49.20	0.49	843.7	453.4	263.9	60.59	0.46	1288.0	897.7	393.1	33.40	0.45
FlashSVD v2	390.3	634.5	244.2	238.1	49.20	0.49	843.7	453.4	396.8	60.63	0.46	1288.0	897.7	744.4	33.42	0.45
FWSVD	390.3	875.4	485.1	110.5	89.29	-	1366.5	976.3	113.7	82.34	-	2374.8	1984.5	220.8	77.21	-
FlashFWSVD	390.3	599.5	209.2	127.4	89.00	0.43	814.7	424.4	217.1	82.11	0.43	1271.1	880.8	401.3	77.46	0.44
Parameter Ratio: 50%																
Vanilla SVD	307.6	790.8	483.3	110.3	50.94	-	1274.0	966.4	100.7	62.07	-	2264.2	1956.7	247.7	31.16	-
FlashSVD v1	307.6	519.4	211.8	148.8	51.34	0.44	731.1	423.5	170.1	62.08	0.44	1178.5	870.9	287.1	31.10	0.45
FlashSVD v2	307.6	519.4	211.8	195.1	51.63	0.44	731.1	423.5	313.7	62.06	0.44	1178.5	870.9	570.8	31.07	0.45
FWSVD	307.6	782.9	475.3	103.0	71.09	-	1266.0	958.5	93.5	63.36	-	2256.1	1948.5	345.6	37.82	-
FlashFWSVD	307.6	511.3	203.7	105.5	69.49	0.43	723.2	415.6	156.7	63.31	0.43	1170.4	862.8	279.2	38.40	0.44

Evaluation Metrics For encoders, we assess model quality via task-specific classification accuracy on widely-recognized GLUE datasets [25], evaluating performance at input lengths of 128, 256, and 512 tokens. Memory efficiency is quantified by measuring peak activation usage during end-to-end inference, and reported in mebibytes (MiB) - using PyTorch’s profiler. Compute efficiency is captured through wall-clock latency per batch (milliseconds) on an NVIDIA L40S GPU. We evaluate a family of models spanning a range of compression ratios ($\frac{\# \text{ Param Compressed}}{\# \text{ Param Dense}}$) divided by that of the dense baseline) and report how latency and memory savings scale as the parameter budget is varied.

5.2. Main Results

Table 2 demonstrates that FlashSVD strikes an outstanding balance between model compression, memory footprint, and inference throughput on both BERT-Base and RoBERTa-Base across multiple GLUE benchmarks. Regardless of the compression ratio, FlashSVD incurs no measurable degradation relative to the vanilla SVD and FWSVD method (maximum difference of only 0.58 % for RoBERTa at 50 % parameters on MNLI). At the same time, it slashes transient activation memory by 69 % on SST-2 and QQP and by 75 % on MNLI, reducing peak inference usage to 1,213 MiB, well below the 1,547 MiB of the original BERT and the 1,990 MiB of a naive SVD, compressed variant. These results reveal that the naive SVD-based compression, despite lowering parameter counts, can actually inflate runtime memory demands and undermine deployment in resource-constrained environments.

Moreover, FlashSVD maintains competitive inference latency while entirely eliminating large dense intermediate tensors, despite the additional I/O tradeoff. On MNLI, with 50 % of the original parameters retained, FlashSVD processes each batch in 341 ms, nearly 20 % faster than the 427.8 ms observed with the baseline SVD approach. Similarly, on SST-2 under the same compression level, FlashSVD achieves 141.6 ms per batch versus 150.8 ms for vanilla SVD. These results demonstrate that our rank-aware optimizations not only preserve model

Table 3: Rank Awareness: latency and transient-memory trade-offs on SST-2 as MHA/FFN rank varies, Sequence Length = 128 for SST-2 dataset and 256 for STS-B dataset

Dataset & Method	MHA Rank	Latency (ms)	Trans. Mem. (MB)	Peak. Mem. (MB)
SST-2 Vanilla SVD ($b = 32$)	64	112.9	214.2	719.6
	56	114.0	214.2	708.6
	48	112.2	214.2	697.7
	32	110.1	214.2	675.7
SST-2 FlashSVD ($b = 32$)	64	166.0	136.5	641.9
	56	165.5	125.2	619.7
	48	164.9	118.2	601.7
	32	158.9	118.2	579.7
STS-B Vanilla SVD ($b = 32$)	768	158.1	424.3	929.7
	384	132.7	413.1	756.5
	192	138.3	406.8	669.2
	96	126.7	404.1	626.0
STS-B FlashSVD ($b = 32$)	768	285.8	250.6	756.0
	384	152.0	251.4	594.8
	192	119.4	251.1	513.5
	96	109.6	251.4	473.3

accuracy and drastically reduce memory consumption but also sustain-and in some cases improve-inference speed relative to both dense and standard SVD-based methods.

In the extreme configuration, FlashSVD achieves comparable memory savings but incurs substantial latency overhead, with up to 60 % in some cases, because the extra reconstruction loop in the feed-forward network undermines parallelism. Although FlashSVDFFN V2 offers a theoretically lower transient memory bound, FlashSVDFFN V1 strikes a more balanced trade-off between memory reduction and inference speed and is therefore the recommended variant for practical deployment.

Rank Awareness As shown in Table 3, in the attention module, as we reduce the SVD rank from 64 to 32, peak activation memory drops from 641.9 MiB to 579.7 MiB, but transient memory levels off at around 118 MiB by rank 48. Beyond this point, other components of the transformer (i.e. residual buffers and layer-norm state) become the dominant contributors to the working set and scaling pattern halted. Latency also falls modestly with rank: FlashSVD’s processing time decreases slightly from 166.0 ms at rank 64 to 158.9 ms at rank 32, a 4.3 % reduction. These observations show that at higher ranks, the $O(BHMr_{\Theta^*})$ low-rank factors dictate memory usage while highlighting that the MHA is not the latency overhead.

In the FFN module, FlashSVDFFN V1 latency steadily improves as the rank shrinks: from 152.0 ms at rank 384 to 119.4 ms at 192 and 109.6 ms at 96 over the vanilla SVD. Throughout this range, transient memory remains essentially constant round 250 MiB, confirming that in medium-to-low rank regimes the MHA components, with memory complexity of $O(BHMr_{\Theta^*})$, remain the primary drivers of the transient memory footprint, and that our rank-aware reconstruction effectively restores parallelism without inflating activation buffers.

5.3. Ablation Study

FlashSVDAttn To quantify the speed-quality trade-offs introduced by our FlashSVDAttn module, we measure relative speedup in latency against PyTorch’s fused SDPA (equivalent to FlashAttention) across mild ($M \leq 256$)

Table 4: STS-B (Pearson) Performance and 50% Compression Ratio with Finetuning

Model	Acc. (%)	Trans. Mem (MiB)	Peak Mem. (MiB)	Lat. (ms)
Dense	81.41	281.3	699.0	98.8
SVD	80.52	399.8	652.8	128.9
FlashSVD	80.52	207.8	460.8	114.8
SVD (no finetune)	13.50	408.3	658.0	160.1

and long ($M \geq 512$) contexts. As shown in Table S3, at full rank ($R = 64$) FlashSVDAttn runs at $0.62\times$ the speed of Dense for $M = 128$ and $0.89\times$ for $M = 256$, but as we reduce rank, the gap narrows: at $R = 32$ the module achieves parity with Dense ($1.00\times$) for $M = 256$, and at $R = 16$ it actually surpasses Dense by 8% ($1.08\times$) in the mild setting. In the compute-bound long-context regime, FlashSVDAttn consistently outperforms Dense—speedups grow from $1.05\times$ at $R = 64$ up to $1.37\times$ ($M = 512$) and $1.64\times$ ($M = 1024$) at $R = 16$. This ablation confirms that (1) low-rank FlashSVDAttn can match or exceed fused SDPA even for medium or short context and (2) delivers substantial speedups for long sequences, validating its practical utility in both regimes.

FlashSVDFFN Table S2 summarizes the computation-efficiency gains of our FlashSVDFFN kernels across a range of FFN truncation ranks and context lengths. FlashSVDFFN V1 offers the best practical trade-off between memory reduction and speedup. At rank 192, FlashSVDFFN V1 achieves over 50% of dense speed for medium (256) contexts and nearly 80% for longer (512–1024). At rank 96, it outperforms dense FFN by up to $1.9\times$, demonstrating that low-rank fusion can turn compression into a net performance gain. FlashSVDFFN V2 follows the same trend but with smaller peak speedups (around $0.25\times$ at rank 96) due to finer-grained tiling limiting parallelism. Overall, FlashSVDFFN V1 strikes the ideal balance-leveraging reduced arithmetic and maintained GPU occupancy - to deliver up to $1.9\times$ acceleration over the dense FFN under realistic low-rank budgets.

Finetuning Unlocks Extreme Low-Rank Compression While many recent methods [30, 27, 10] emphasize training-free SVD to avoid retraining overhead, our results show that judicious fine-tuning of low-rank factors unleashes far greater compression without accuracy loss. In particular, by fine-tuning BERT after 50% parameter reduction, we recover nearly full task performance while slashing transient memory by 48.2% and peak memory by 29.4%, about same size as the persistent memory of dense model (Table 4). These findings underscore that a rank-aware inference framework, like FlashSVD, paired with targeted fine-tuning can push transformer models to much more aggressive low-rank regimes, making extreme compression truely viable for edge deployment with minimal performance loss. Full details is available in table S6.

6. Conclusion

In this work, we introduce FlashSVD, the first fused, rank-aware inference framework for SVD-compressed transformers. By streaming low-rank projections directly into FlashAttention and FFN kernels, we eliminate large activations and cut peak on-chip memory by up to 71% with no extra computational cost. Across BERT and RoBERTa, FlashSVD matches or exceeds dense throughput under 25–50% compression and achieves up to $1.9\times$ FFN speedups at modest ranks. These results demonstrate that rank-aware tiling makes low-rank SVD a practical, high-performance strategy for memory-constrained transformer deployment.

References

- [1] C.-C. Chang, W.-C. Lin, C.-Y. Lin, C.-Y. Chen, Y.-F. Hu, P.-S. Wang, N.-C. Huang, L. Ceze, M. S. Abdelfattah, and K.-C. Wu. Palu: KV-cache compression with low-rank projection. In *The Thirteenth International Conference on Learning Representations*, 2025. URL <https://openreview.net/forum?id=LWMS4pk2vK>.
- [2] T. Dao, D. Y. Fu, S. Ermon, A. Rudra, and C. Ré. Flashattention: Fast and memory-efficient exact attention with io-awareness. *arXiv preprint*, 2022. arXiv:2205.14135.
- [3] T. Dao, D. Y. Fu, S. Ermon, A. Rudra, and C. Ré. Flashattention-2: Faster attention with better parallelism and work partitioning. *arXiv preprint*, 2023. arXiv:2307.08691.
- [4] T. Dettmers, A. Pagnoni, A. Holtzman, and L. Zettlemoyer. Qlora: Efficient finetuning of quantized llms. *arXiv preprint*, 2023. arXiv:2305.14314.
- [5] J. Devlin, M.-W. Chang, K. Lee, and K. Toutanova. Bert: Pre-training of deep bidirectional transformers for language understanding. In *Proceedings of the 2019 conference of the North American chapter of the association for computational linguistics: human language technologies, volume 1 (long and short papers)*, pages 4171–4186, 2019.
- [6] C. Eckart and G. Young. The approximation of one matrix by another of lower rank. *Psychometrika*, 1(3): 211–218, 1936.
- [7] A. Gordon, E. Eban, O. Nachum, B. Chen, H. Wu, T.-J. Yang, and E. Choi. Morphnet: Fast & simple resource-constrained structure learning of deep networks. *arXiv preprint arXiv:1711.06798*, 2017.
- [8] S. Han, H. Mao, and W. J. Dally. Deep compression: Compressing deep neural networks with pruning, trained quantization and huffman coding. In *International Conference on Learning Representations (ICLR)*, 2016. arXiv:1510.00149.
- [9] Y. He, X. Zhang, and J. Sun. Channel pruning for accelerating very deep neural networks. In *IEEE International Conference on Computer Vision (ICCV)*, Oct 2017.
- [10] Y.-C. Hsu, T. Hua, S. Chang, Q. Lou, Y. Shen, and H. Jin. Language model compression with weighted low-rank factorization. *arXiv preprint arXiv:2207.00112*, 2022.
- [11] E. J. Hu, Y. Shen, P. Wallis, Z. Allen-Zhu, Y. Li, S. Wang, L. Wang, and W. Chen. Lora: Low-rank adaptation of large language models. In *ICLR*, 2021. arXiv:2106.09685.
- [12] B. Jacob, S. Kligys, B. Chen, M. Zhu, M. Tang, A. Howard, H. Adam, and D. Kalenichenko. Quantization and training of neural networks for efficient integer-arithmetic-only inference. In *Proceedings of the IEEE/CVF Conference on Computer Vision and Pattern Recognition (CVPR)*, pages 2704–2713, 2018. arXiv:1712.05877.
- [13] H. Li, A. Kadav, I. Durdanovic, H. Samet, and H. P. Graf. Pruning filters for efficient convnets. In *International Conference on Learning Representations (ICLR)*, 2017. arXiv:1608.08710.
- [14] B. Lin and Colleagues. Modegpt: Modular decomposition for large language model compression. In *ICML*, 2024. OpenReview: 8EfxjTCg2k.

- [15] S. Lin, R. Ji, Y. Li, C. Deng, and X. Li. Towards compact convnets via structure-sparsity regularized filter pruning. *arXiv preprint arXiv:1901.07827*, 2019.
- [16] F. Liu and N. Team. Star attention: Efficient llm inference over long sequences. arXiv preprint, 2024. arXiv:2411.17116.
- [17] Y. Liu, M. Ott, N. Goyal, J. Du, M. Joshi, D. Chen, O. Levy, M. Lewis, L. Zettlemoyer, and V. Stoyanov. Roberta: A robustly optimized bert pretraining approach. *arXiv preprint arXiv:1907.11692*, 2019.
- [18] J.-H. Luo and J. Wu. An entropy-based pruning method for cnn compression. *arXiv preprint arXiv:1706.05791*, 2017.
- [19] J.-H. Luo, J. Wu, and W. Lin. Thinet: A filter level pruning method for deep neural network compression. In *IEEE International Conference on Computer Vision (ICCV)*, 2017. arXiv:1707.06342.
- [20] R. Pope, S. Douglas, A. Chowdhery, J. Devlin, J. Bradbury, J. Heek, K. Xiao, S. Agrawal, and J. Dean. Efficiently scaling transformer inference. *Proceedings of Machine Learning and Systems*, 5:606–624, 2023.
- [21] J. Shah, G. Bikshandi, Y. Zhang, V. Thakkar, P. Ramani, and T. Dao. Flashattention-3: Fast and accurate attention with asynchrony and low-precision. *Advances in Neural Information Processing Systems*, 37: 68658–68685, 2024.
- [22] E. Shi and Team. Blockllm: Multi-tenant finer-grained serving for large language models. arXiv preprint, 2024. arXiv:2404.18322.
- [23] M. Shoeybi, M. Patwary, R. Puri, P. LeGresley, J. Casper, and B. Catanzaro. Megatron-lm: Training multi-billion parameter language models using model parallelism. *arXiv preprint arXiv:1909.08053*, 2019.
- [24] H. Touvron, T. Lavril, G. Izacard, X. Martinet, M.-A. Lachaux, T. Lacroix, B. Rozière, N. Goyal, E. Hambro, F. Azhar, et al. Llama: Open and efficient foundation language models. *arXiv preprint arXiv:2302.13971*, 2023.
- [25] A. Wang, A. Singh, J. Michael, F. Hill, O. Levy, and S. R. Bowman. Glue: A multi-task benchmark and analysis platform for natural language understanding. *arXiv preprint arXiv:1804.07461*, 2018.
- [26] Q. Wang, J. Ke, M. Tomizuka, K. Keutzer, and C. Xu. Dobi-svd: Differentiable svd for llm compression and some new perspectives. In *ICLR*, 2025. OpenReview: kws76i5XB8.
- [27] X. Wang, Y. Zheng, Z. Wan, and M. Zhang. Svd-llm: Truncation-aware singular value decomposition for large language model compression. *arXiv preprint arXiv:2403.07378*, 2024.
- [28] X. Wang, S. Alam, Z. Wan, H. Shen, and M. Zhang. Svd-llm v2: Optimizing singular value truncation for large language model compression. *arXiv preprint arXiv:2503.12340*, 2025.
- [29] H. Wu, P. Judd, X. Zhang, M. Isaev, and P. Micikevicius. Integer quantization for deep learning inference: Principles and empirical evaluation. *arXiv preprint arXiv:2004.09602*, 2020.
- [30] A. Yuan and Others. Activation-aware singular value decomposition for large language models. OpenReview preprint, 2023. arXiv:2502.01403.

- [31] J. Zhang, Y. Zhang, J. Gu, J. Dong, L. Kong, and X. Yang. Xformer: Hybrid x-shaped transformer for image denoising. In *ICLR*, 2024.
- [32] S. Zhang, S. Roller, N. Goyal, M. Artetxe, M. Chen, S. Chen, C. Dewan, M. Diab, X. Li, X. V. Lin, et al. Opt: Open pre-trained transformer language models. *arXiv preprint arXiv:2205.01068*, 2022.

Algorithm S1 FlashSVDFFN Forward Pass V2

Require: Input $X \in \mathbb{R}^{B \times M \times \mathcal{D}_{\mathcal{A}}^{\Theta}}$; SVD factors $U_i \in \mathbb{R}^{\mathcal{D}_{\mathcal{A}}^{\Theta} \times r_{\Theta^*}}$, $V_i \in \mathbb{R}^{r_{\Theta^*} \times \mathcal{D}_{\mathcal{F}}^{\Theta}}$, $b_i \in \mathbb{R}^{\mathcal{D}_{\mathcal{F}}^{\Theta}}$;
 $U_o \in \mathbb{R}^{\mathcal{D}_{\mathcal{F}}^{\Theta} \times r_{\Theta^*}}$, $V_o \in \mathbb{R}^{r_{\Theta^*} \times \mathcal{D}_{\mathcal{A}}^{\Theta}}$, $b_o \in \mathbb{R}^{\mathcal{D}_{\mathcal{A}}^{\Theta}}$; number of blocks G ; nonlinearity $\phi(\cdot)$.

Ensure: $O \in \mathbb{R}^{B \times M \times \mathcal{D}_{\mathcal{A}}^{\Theta}}$

```

1:  $B_M \leftarrow \lceil M/G \rceil$ ,  $B_{D_{\mathcal{F}}^{\Theta}} \leftarrow \lceil \mathcal{D}_{\mathcal{F}}^{\Theta}/G \rceil$ 
2: Initialize  $O \leftarrow 0_{B \times M \times \mathcal{D}_{\mathcal{A}}^{\Theta}}$ ,  $Z_{\text{tile}} \leftarrow 0_{B \times B_M \times \mathcal{D}_{\mathcal{A}}^{\Theta}}$ 
3: On-Chip: direct activation streaming
4: for  $\ell = 0$  to  $M - 1$  step  $B_M$  do
5:    $P_{\text{tile}} \leftarrow X[:, \ell : \ell + B_M, :] U_i[:, k] \{(B, B_M, r_{\Theta^*})\}$ 
6:   for  $d = 0$  to  $\mathcal{D}_{\mathcal{F}}^{\Theta} - 1$  step  $B_{D_{\mathcal{F}}^{\Theta}}$  do
7:     for  $k = 0$  to  $r_{\Theta^*} - 1$  do
8:        $Y += P_{\text{tile}} V_i[k, d : d + B_{D_{\mathcal{F}}^{\Theta}}]$ 
9:     end for
10:     $Y \leftarrow \phi(Y + b_i[d : d + B_{D_{\mathcal{F}}^{\Theta}}]) \{(B \times B_M \times \mathcal{D}_{\mathcal{F}}^{\Theta})\}$ 
11:    for  $k = 0$  to  $r_{\Theta^*} - 1$  do
12:       $Z_{\text{tile}} += Y U_o[d : d + B_{D_{\mathcal{F}}^{\Theta}}, k] + b_o[d : d + B_{D_{\mathcal{F}}^{\Theta}}]$ 
13:    end for
14:  end for
15: end for
16:  $O \leftarrow Z_{\text{tile}}$  accumulation  $\{\text{broadcast to } (B, B_M, \mathcal{D}_{\mathcal{A}}^{\Theta})\}$ 

```

S1. Supplementary Materials

S2. Appendix

S2.1. Additional Methodology

FlashSVDFFN V2 (Extreme-Case) The FFN kernel streams low-rank factors of both weight matrices $W_i^{[r_{\Theta^*}]} = U_i \Sigma_i V_i$ and $W_o^{[r_{\Theta^*}]} = U_o \Sigma_o V_o$ through a fused GEMM–ACTIVATION–GEMM pipeline on arbitrary activation function $\phi(\cdot)$. We tile the sequence dimension into chunks of batch-sequence dimension B_M and the intermediate feature dimension $\mathcal{D}_{\mathcal{F}}^{\Theta}$ into blocks of width $B_{D_{\mathcal{F}}^{\Theta}}$. For each $(B \times B_M) \times B_{D_{\mathcal{F}}^{\Theta}}$ tile:

$$Y = \phi((X_{\text{tile}} U_i) V_{i,\text{tile}}), \quad Z_{\text{tile}} += (Y U_{o,\text{tile}}) V_o,$$

where $(\cdot)_{\text{tile}}$ denotes the accumulation buffer on SRAM. By launching one kernel block per tile and accumulating directly into the output buffer, we avoid any materialized $(B \times M) \times \mathcal{D}_{\mathcal{F}}^{\Theta}$ mid-buffers, achieving the $O(r_{\Theta^*}(B M + \mathcal{D}_{\mathcal{F}}^{\Theta}))$ HBM bound of Theorem 9.

FlashSVDFFN V2 (Alg. S1) incurs no additional arithmetic cost or asymptotic complexity compared to a dense FFN: it executes the identical $O(B M r_{\Theta^*} \mathcal{D}_{\mathcal{F}}^{\Theta} + B M r_{\Theta^*} \mathcal{D}_{\mathcal{A}}^{\Theta})$ FLOPs, yet reduces peak on-chip storage per token from $O(r_{\Theta^*}(B M + \mathcal{D}_{\mathcal{F}}^{\Theta}))$ to $O(r_{\Theta^*} \mathcal{D}_{\mathcal{F}}^{\Theta})$. This theoretically pushes the lower bound for variable part of rank-aware activation compression to zero (see Theorem 10). In practice, however, V2’s fine-granularity tiling can limit GPU parallelism, especially in higher rank case, and our experiments show that factors such as residual-add operation and layer-norm ordering begin to dominate end-to-end latency. Addressing these secondary bottlenecks will be key to unlocking V2’s full on-edge performance potential.

	$\mathcal{D}_{\mathcal{A}}^{\Theta}$	H	$d_{\Theta_{\mathcal{A}},h}$	Threshold on r
Multi-Head	768	12	64	$r < \frac{768}{13} \approx 59.1$
Single Head	768	—	—	$r < \frac{768}{2} = 384$

Table S1: Example (BERT-Base, $\mathcal{D}_{\mathcal{A}}^{\Theta} = 768$, $H = 12$, $d_{\Theta_{\mathcal{A}},h} = \mathcal{D}_{\mathcal{A}}^{\Theta}/H$): Rank-truncation thresholds for head-wise vs. full-matrix SVD to achieve compression.

Proof of MHA Reduction Efficiency We provide the proof of rank-loss efficiency for the MHA based compression. We have also provided a case study with results summarized in table S1.

Proof. Given $\mathcal{D}_{\mathcal{A}}^{\Theta} = d_{\Theta_{\mathcal{A}},h} \times H$, the SVD for single head projection matrices $W_a \in \mathbb{R}^{\mathcal{D}_{\mathcal{A}}^{\Theta} \times \mathcal{D}_{\mathcal{A}}^{\Theta}}$, $\forall a \in q, k, v$, we have $W_a = U_a V_a$ in full rank case, which $U_a V_a \in \mathbb{R}^{\mathcal{D}_{\mathcal{A}}^{\Theta} \times r_{\Theta^*}}$. Once $r_{\Theta^*} = \mathcal{D}_{\mathcal{A}}^{\Theta}$, we have $U_a V_a$ be twice larger than W_a and we can only achieve compression after pruning over half of the rank. For multi-head case, which $W_a = \bigcup_{h=1}^H W_a^{(h)}$, $\forall h \in 1, 2, \dots, H$ and $W_a^{(h)} \in \mathbb{R}^{\mathcal{D}_{\mathcal{A}}^{\Theta} \times d_{\Theta_{\mathcal{A}},h}}$. The low-rank decomposition is given as $W_a^{(h)} \approx U_a^{(h)} V_a^{(h)}$, with $U_a^{(h)} \in \mathbb{R}^{\mathcal{D}_{\mathcal{A}}^{\Theta} \times r_{\Theta^*}}$ and $V_a^{(h)} \in \mathbb{R}^{r_{\Theta^*} \times d_{\Theta_{\mathcal{A}},h}}$ with $r_{\Theta^*} \leq d_{\Theta_{\mathcal{A}},h}$. Therefore, in the worst case where $r_{\Theta^*} = d_{\Theta_{\mathcal{A}},h}$, we have $\bigcup_{h=1}^H \left(U_a^{(h)} V_a^{(h)} \right)$ in size:

$$\begin{aligned}
& H \times \mathcal{D}_{\mathcal{A}}^{\Theta} \times d_{\Theta_{\mathcal{A}},h} + H \times d_{\Theta_{\mathcal{A}},h} \times d_{\Theta_{\mathcal{A}},h} \\
&= H \times \mathcal{D}_{\mathcal{A}}^{\Theta} \times d_{\Theta_{\mathcal{A}},h} + \mathcal{D}_{\mathcal{A}}^{\Theta} \times d_{\Theta_{\mathcal{A}},h} \\
&= (H + 1) \times \mathcal{D}_{\mathcal{A}}^{\Theta} \times d_{\Theta_{\mathcal{A}},h}
\end{aligned}$$

Thus, it only requires $r_{\Theta^*} < \frac{1}{2} \mathcal{D}_{\mathcal{A}}^{\Theta}$, rank reduction to achieve parameter reduction benefits in comparison to $r_{\Theta^*} < \frac{1}{2} \mathcal{D}_{\mathcal{A}}^{\Theta}$, of single head case. \square

Palu [1] showed that grouping H heads into G -SVD blocks improves the reconstruction-expressivity trade-off in the KV-Cache of low-rank models; Theorem 7 and Proposition 6 extends this to general compression of model weights and activations (e.g. Q, K, V, FFN intermediates, attention output projection) at cost $\mathcal{O}\left(G r_{\Theta^*} (B M + \frac{\mathcal{D}_{\mathcal{A}}^{\Theta}}{G})\right)$, interpolating between $G = 1$ and $G = H$. Moreover, we apply this analysis uniformly to transformer layers and, for the first time, quantify its impact on peak activation memory.

S2.2. Additional Analysis

In this section, we characterize FlashSVD’s advantages under practical modeling conditions. We begin by deriving tight memory-complexity bounds for low-rank activations, explicitly comparing against both full-rank storage and naive low-rank implementations. Building on this foundation, we introduce a layer-wise sensitivity analysis that reveals which parts of the Transformer—be it multi-head attention, grouped-head attention, or the feed-forward network—yield the greatest benefit per truncated singular dimension. We then turn to computational costs, providing detailed estimates of FLOP reductions and end-to-end kernel latency improvements. Finally, we establish provable bounds on the numerical error introduced by streaming, showing how metrics such as perplexity degrade as a function of rank, layer depth, and data distribution. All main statements are formalized as theorems or lemmas, with proof sketches deferred to the appendix.

S2.3. Memory Complexity

For any given model Θ , let $X \in \mathbb{R}^{B \times M \times \mathcal{D}_{\mathcal{A}}^{\Theta}}$ denote a batch of B token sequences of length M with hidden dimensionality $\mathcal{D}_{\mathcal{A}}^{\Theta}$. In both training and inference, a Transformer's memory consumption is dominated by (i) the static storage of its model parameters and (ii) the dynamic allocations required to hold intermediate activations. In particular, the activations for the attention sublayer consist of the query, key, and value tensors $Q, K, V \in \mathbb{R}^{B \times M \times \mathcal{D}_{\mathcal{A}}^{\Theta}}$, while the feed-forward sublayer produces $S_{\text{out}} \in \mathbb{R}^{B \times M \times \mathcal{D}_{\mathcal{F}}^{\Theta}}$, where $\mathcal{D}_{\mathcal{F}}^{\Theta}$ denotes the hidden dimension of the intermediate projection. In this work, we propose replacing each of these full-rank activation tensors with a rank- r approximation computed via singular value decomposition (SVD). We derive upper bounds on the resulting memory footprint—showing that it scales as $\mathcal{O}(r_{\Theta^*}(BM + \mathcal{D}_{\mathcal{A}}^{\Theta} + \mathcal{D}_{\mathcal{F}}^{\Theta}))$ rather than $\mathcal{O}(BMD_{\mathcal{A}}^{\Theta} + BMD_{\mathcal{F}}^{\Theta})$ —and we quantify the trade-off between compression ratio and approximation error. This theoretical analysis lays the groundwork for deploying rank-constrained Transformers in resource-limited settings without sacrificing accuracy.

Remark 1 (Scope of Memory Analysis). *Throughout the following off-chip memory analyses, we focus on the variable (change-inducing) components and omit persistent peak memory terms, such as the HBM-resident matrices $V_* \in \mathbb{R}^{r_{\Theta^*} \times \mathcal{D}_{\mathcal{A}}^{\Theta}}$ and the final output activations. However, when discussing rank selection and practical deployment guidance, we account for the full off-chip memory footprint, including both transient and persistent terms, to ensure our analysis reflects real-world constraints. Note that we conduct memory analysis at the per-layer level, excluding the output activation $\mathbb{R}^{B \times M \times \mathcal{D}_{\mathcal{A}}^{\Theta}}$ and $\mathbb{R}^{B \times M \times \mathcal{D}_{\mathcal{F}}^{\Theta}}$, which is always present and agnostic to the attention variant.*

Attention We first consider the multi-head attention module in a Transformer block, which is parameterized by the projection matrices $W_q, W_k, W_v \in \mathbb{R}^{\mathcal{D}_{\mathcal{A}}^{\Theta} \times \mathcal{D}_{\mathcal{A}}^{\Theta}}$ and applied to an input of shape $(B, M, \mathcal{D}_{\mathcal{A}}^{\Theta})$. When the total activation size BM far exceeds the hidden dimension $\mathcal{D}_{\mathcal{A}}^{\Theta}$, the DRAM footprint of the query, key, value, and scoring tensors typically dominates. In what follows, we derive tight upper and lower bounds on the off-chip memory cost incurred by SVD-based compression of these attention activations.

Definition 1 (Attention Activation Approximation). *Let $X \in \mathbb{R}^{B \times M \times \mathcal{D}_{\mathcal{A}}^{\Theta}}$ be the input to a multi-head attention block with projection matrices $W_q, W_k, W_v \in \mathbb{R}^{\mathcal{D}_{\mathcal{A}}^{\Theta} \times \mathcal{D}_{\mathcal{A}}^{\Theta}}$. Define the (flattened) query, key, and value activations $Q = XW_q, K = XW_k, V = XW_v$, each of shape $\mathbb{R}^{(BM) \times \mathcal{D}_{\mathcal{A}}^{\Theta}}$. We say that Q admits a rank- r SVD approximation if*

$$Q^{[r_{\Theta}^*]} = U_Q \Sigma_Q V_Q^{\top}, \quad (S1)$$

$$U_Q \in \mathbb{R}^{(BM) \times r_{\Theta}^*}, \quad \Sigma_Q \in \mathbb{R}^{r_{\Theta}^* \times r_{\Theta}^*}, \quad V_Q \in \mathbb{R}^{\mathcal{D}_{\mathcal{A}}^{\Theta} \times r_{\Theta}^*}.$$

and similarly for K and V , with r_{Θ}^* be the layer rank given by the compression algorithm. Compressing all three projections to rank r then replaces the full activations by the factor pairs (U_Q, Σ_Q, V_Q) , (U_K, Σ_K, V_K) , and (U_V, Σ_V, V_V) , which the Σ_* are usually merged into either U_* or V_* for simplicity.

For a Transformer layer $\Theta_{\mathcal{A}}$ with H attention heads, the total attention dimension $\mathcal{D}_{\mathcal{A}}^{\Theta}$ is uniformly partitioned across heads, so each head has dimension

$$d_{\Theta_{\mathcal{A}}, h} := \frac{\mathcal{D}_{\mathcal{A}}^{\Theta}}{H}.$$

All activation tensors $(Q, K, V) \in \mathbb{R}^{B \times M \times \mathcal{D}_{\mathcal{A}}^{\Theta}}$ are reshaped as H parallel sub-tensors of shape $\mathbb{R}^{B \times M \times d_{\Theta_{\mathcal{A}}, h}}$ to enable independent attention computations per head.

Theorem 1 (Memory Complexity of Dense Multi-Head Attention). *For a single-head attention module defined in Definition 1, the peak working memory (number of stored scalars) required by the unoptimized dense multi-head attention mechanism is $\mathcal{M}_{\text{dense}} = 3 B M \mathcal{D}_{\mathcal{A}}^{\Theta} + B M^2$.*

Proof. In the standard dense Θ and unoptimized low-rank model Θ^* , one first computes three full-rank linear projections of the input embeddings into queries Q , keys K , and values V . Each of these tensors has shape $B \times M \times \mathcal{D}_{\mathcal{A}}^{\Theta}$, and to avoid redundant re-computation all three must reside in memory simultaneously, contributing

$$\sum_{a \in \{q, k, v\}} B M \mathcal{D}_{\mathcal{A}}^{\Theta} = 3 B M \mathcal{D}_{\mathcal{A}}^{\Theta}.$$

Next, the attention logits are formed as the batch of pairwise dot-product matrices

$$S^{(b)} = Q^{(b)} K^{(b) \top} \quad \text{for } b = 1, \dots, B,$$

each of size $M \times M$. Storing all B score matrices therefore requires $B M^2$ scalars. No other intermediate buffers exceed these sizes, so the total peak memory is $\mathcal{M}_{\text{dense}} = 3 B M \mathcal{D}_{\mathcal{A}}^{\Theta} + B M^2$. \square

Proposition 1 (Memory Complexity of Multi-Head Attention). *A multi-head attention module defined in Definition 1 yields a total dense attention memory cost $\mathcal{M}_{\text{dense}} = \mathcal{O}(B M \mathcal{D}_{\mathcal{A}}^{\Theta} + H B M^2)$.*

Proof. Each head computes its own set of projections for queries, keys, and values, each of shape $B \times M \times d_{\Theta_{\mathcal{A}}, h}$, where $d_{\Theta_{\mathcal{A}}, h} = \mathcal{D}_{\mathcal{A}}^{\Theta} / H$. Across all heads, the total Q , K , V memory remains as stated in Theorem 1:

$$\mathcal{M}_{QKV} = 3 B M \mathcal{D}_{\mathcal{A}}^{\Theta}.$$

Each head also computes a score matrix of shape $B \times M \times M$, contributing $B M^2$ memory per head. With H heads, these score matrices total:

$$\mathcal{M}_{\text{scores}} = H B M^2.$$

Therefore, the total dense memory cost is:

$$\mathcal{M}_{\text{dense}} = 3 B M \mathcal{D}_{\mathcal{A}}^{\Theta} + H B M^2.$$

\square

To mitigate the high memory overhead of materializing the full $B M^2$ attention score matrix, we adopt FlashAttention [2, 3], which streams the computation and avoids instantiating intermediate tensors. The following proposition quantifies its peak memory usage.

Proposition 2 (Memory Complexity with FlashAttention). *Under the same notation in Proposition 1, the peak HBM footprint of streaming (Flash) attention is*

$$\mathcal{M}_{\text{flash-attn}} = 3 B M \mathcal{D}_{\mathcal{A}}^{\Theta},$$

as the $\mathcal{O}(B M^2)$ score-matrix never coexists in off-chip memory.

Proof. FlashAttention partitions the M -length sequence into tiles whose keys and values are loaded on-chip (in SRAM) just long enough to compute the corresponding query-key dot-products. Queries stream through the device once, accumulating weighted sums of values, and each key and value tile is evicted immediately after use. As a result, only the three $B \times M \times \mathcal{D}_{\mathcal{A}}^{\Theta}$ projections (for Q, K, V) occupy HBM simultaneously, yielding $\mathcal{M}_{\text{flash}} = 3 B M \mathcal{D}_{\mathcal{A}}^{\Theta}$. \square

Despite low-rank compression of the attention weights, standard attention implementations still require reconstructing full Q , K , and V tensors, leading to quadratic memory costs. This limitation is formalized below.

Proposition 3 (Activation Materialization Lower Bound). *Vanilla SVD models Θ^* defined in Definition 1 requires dense formulation of Q, K, V despite the weights W_q, W_k, W_v are offloaded in low-rank formats $U_{q,k,v} \in \mathbb{R}^{B \times M \times r_{\Theta^*}}$ and $V_{q,k,v} \in \mathbb{R}^{r_{\Theta^*} \times \mathcal{D}_{\mathcal{A}}^{\Theta}}$. Therefore, a standard attention implementation requires reconstructing full $\mathbb{R}^{B \times M \times \mathcal{D}_{\mathcal{A}}^{\Theta}}$ tensors, so peak dynamic memory remains $O(BHM^2)$.*

Proof. Storing factors ($U_{q,k,v} \in \mathbb{R}^{BM \times r_{\Theta^*}}$, $V_{q,k,v} \in \mathbb{R}^{r_{\Theta^*} \times \mathcal{D}_{\mathcal{A}}^{\Theta}}$) uses $(BM + \mathcal{D}_{\mathcal{A}}^{\Theta}) r_{\Theta^*}$ entries. Despite the low-rank parameterization, the full $O(BM \times M)$ score matrix across all heads must be materialized in HBM during a vanilla attention computation, incurring a memory cost of at least $O(BHM^2)$. \square

Although current GPU constraints prevent applying FlashSVD directly to single-head attention due to unsupported kernel tiling, and real-world memory behavior remains governed by Proposition 2, we nevertheless provide a complete theoretical analysis in Theorems 2 and 3, with further rank sensitivity characterized in Proposition 4.

Theorem 2 (Memory Complexity of FlashSVDAttention). *Consider a low-rank attention model Θ^* with factorization rank r_{Θ^*} . For each $a \in \{q, k, v\}$, the projection matrix W_a is decomposed as $W_a = P_a V_a$, where $P_a = X U_a$ with $X \in \mathbb{R}^{B \times M \times \mathcal{D}_{\mathcal{A}}^{\Theta}}$ and $U_a \in \mathbb{R}^{\mathcal{D}_{\mathcal{A}}^{\Theta} \times r_{\Theta^*}}$. Then $P_a \in \mathbb{R}^{B \times M \times r_{\Theta^*}}$ and $V_a \in \mathbb{R}^{r_{\Theta^*} \times \mathcal{D}_{\mathcal{A}}^{\Theta}}$. Under the FlashAttention tiling scheme, the peak variable off-chip memory usage is*

$$M_{\text{flash-svd-attn}} = O(BMr_{\Theta^*}).$$

Proof. According to Remark 1, we focus only on the variable off-chip memory terms whose sizes depend on the batch size B and sequence length M . FlashAttention avoids materializing the full $B \times M \times \mathcal{D}_{\mathcal{A}}^{\Theta}$ projections on HBM. Instead, it streams Q , K , and V through SRAM tile by tile. Thus, the full activation tensors never exist simultaneously off-chip.

The only HBM-resident quantities that vary with the input are the intermediate projections P_a for $a \in \{q, k, v\}$, each with shape $B \times M \times r_{\Theta^*}$. Therefore, across all three projections, the total peak variable HBM memory is

$$\sum_{a \in \{q, k, v\}} BMr_{\Theta^*} = 3BMr_{\Theta^*} = O(BMr_{\Theta^*}).$$

We note that the output-side factors $V_a \in \mathbb{R}^{r_{\Theta^*} \times \mathcal{D}_{\mathcal{A}}^{\Theta}}$ are persistent parameters and not included in the asymptotic result per Remark 1. However, they do contribute a constant offset of $3r_{\Theta^*}\mathcal{D}_{\mathcal{A}}^{\Theta}$ to HBM usage.

In scenarios where $\mathcal{D}_{\mathcal{A}}^{\Theta} \gg M$, the persistent off-chip memory required to store the projection matrices $V_a \in \mathbb{R}^{r_{\Theta^*} \times \mathcal{D}_{\mathcal{A}}^{\Theta}}$ may dominate the total memory footprint, even though the variable memory remains at $O(BMr_{\Theta^*})$. Conversely, in regimes where $\mathcal{D}_{\mathcal{A}}^{\Theta} \ll M$, the dynamic (activation-related) term dominates, and the persistent cost becomes negligible.

\square

Theorem 3 (Single-Head Compression Threshold). *For a single-head attention module defined in Definition 1, low-rank compression yields memory savings if and only if*

$$r_{\Theta^*} < \frac{BMD_{\mathcal{A}}^{\Theta}}{BM + \mathcal{D}_{\mathcal{A}}^{\Theta}}.$$

The maximum achievable compression ratio, attained in the rank-one case $r_{\Theta^} = 1$, is $O(\min\{BM, \mathcal{D}_{\mathcal{A}}^{\Theta}\})$.*

Proof. From Proposition 2, the off-chip memory required by standard FlashAttention is $O(BM\mathcal{D}_{\mathcal{A}}^{\Theta})$.

In contrast, Theorem 2 establishes that FlashSVDAttention requires

$$\mathcal{M}_{\text{flash-svd-attn-single}} = BMr_{\Theta^*} + r_{\Theta^*}\mathcal{D}_{\mathcal{A}}^{\Theta} \quad (\text{for a single head}),$$

which corresponds to the transient peak memory during computation, as clarified in Remark 1.

Memory savings occur when this quantity is smaller than the baseline:

$$BMr_{\Theta^*} + r_{\Theta^*}\mathcal{D}_{\mathcal{A}}^{\Theta} < BM\mathcal{D}_{\mathcal{A}}^{\Theta}.$$

Solving for r_{Θ^*} yields the threshold:

$$r_{\Theta^*} < \frac{BM\mathcal{D}_{\mathcal{A}}^{\Theta}}{BM + \mathcal{D}_{\mathcal{A}}^{\Theta}}.$$

In the extreme low-rank case $r_{\Theta^*} = 1$, the compression ratio becomes

$$\frac{BM\mathcal{D}_{\mathcal{A}}^{\Theta}}{BM + \mathcal{D}_{\mathcal{A}}^{\Theta}},$$

which scales as $O(\min\{BM, \mathcal{D}_{\mathcal{A}}^{\Theta}\})$, depending on which term dominates in the denominator. \square

Proposition 4 (Marginal Memory Reduction per Rank). *Under the same setup as Theorem 3, decreasing the SVD rank from r_{Θ^*} to $r_{\Theta^*} - 1$ reduces the off-chip memory by exactly*

$$\Delta\mathcal{M}_{\text{flash-svd-attn-single}} = O(BM + \mathcal{D}_{\mathcal{A}}^{\Theta}).$$

In particular, each unit drop in rank saves $BM + \mathcal{D}_{\mathcal{A}}^{\Theta}$ elements of HBM storage across the three projections.

Proof. By Theorem 2, the total HBM cost for one head of rank r is

$$\mathcal{M}(r) = O(BM r + r\mathcal{D}_{\mathcal{A}}^{\Theta}).$$

Hence

$$\mathcal{M}(r_{\Theta^*}) - \mathcal{M}(r_{\Theta^*} - 1) = O(BM + \mathcal{D}_{\mathcal{A}}^{\Theta}),$$

which establishes the claimed marginal saving. \square

We now begin our analysis of multi-head attention, which corresponds directly to the implementation in Algorithm 1. The following theorem establishes the transient memory complexity under low-rank compression applied independently to each head.

Theorem 4 (Compressed Multi-Head Memory Upper Bound). *Let a multi-head attention module be defined as in Definition 1, with H heads each operating on activation size $BM \times d_{\Theta_{\mathcal{A}},h}$, where $d_{\Theta_{\mathcal{A}},h} = \mathcal{D}_{\mathcal{A}}^{\Theta}/H$. If each head is compressed to rank r_{Θ^*} , then the total transient off-chip memory reduces from*

$$O(BM\mathcal{D}_{\mathcal{A}}^{\Theta}) \quad \text{to} \quad O(Hr_{\Theta^*}(BM + d_{\Theta_{\mathcal{A}},h})).$$

In particular, setting $r_{\Theta^} = 1$ yields an H -fold memory reduction in the transient term.*

Proof. Each uncompressed attention head requires storing the activation tensor of shape $B M \times d_{\Theta, h}$, for a total of $B M d_{\Theta, h}$ entries. Across all H heads, this yields a total memory of $\mathcal{O}(B M \mathcal{D}_{\mathcal{A}}^{\Theta})$.

Under rank- r_{Θ^*} SVD compression, each head's activation is replaced by two factors of shape $B M \times r_{\Theta^*}$ and $d_{\Theta, h} \times r_{\Theta^*}$, storing

$$(B M + d_{\Theta, h}) \cdot r_{\Theta^*}$$

entries per head. Summing over all heads gives the total

$$H r_{\Theta^*} (B M + d_{\Theta, h}) = H B M r_{\Theta^*} + r_{\Theta^*} \mathcal{D}_{\mathcal{A}}^{\Theta},$$

as claimed.

Finally, we note by Remark 1 that this expression captures only the change-inducing (transient) memory terms. Persistent memory components such as the low-rank bases $V_* \in \mathbb{R}^{r_{\Theta^*} \times \mathcal{D}_{\mathcal{A}}^{\Theta}}$ are not included here, but are considered in total memory budget discussions, e.g., for rank selection. \square

Proposition 5 (Marginal Memory Reduction per Rank in Multi-Head Setting). *Under the setup of Theorem 4, decreasing the SVD rank of each head from r_{Θ^*} to $r_{\Theta^*} - 1$ reduces off-chip memory by*

$$\Delta \mathcal{M}_{\text{flash-svd-attn-multi}} = \mathcal{O}(H (B M + d_{\Theta, h})),$$

In other words, each unit decrease in rank saves $H (B M + d_{\Theta, h})$ elements of DRAM storage across all heads.

Proof. By Theorem 4, the HBM storage cost for multi-head of rank r is

$$\mathcal{M}_{\text{flash-svd-attn-multi}}(r) = \mathcal{O}(H r (B M + d_{\Theta, h})).$$

Hence

$$\begin{aligned} \Delta \mathcal{M}_{\text{flash-svd-attn-multi}} &= \mathcal{M}_{\text{flash-svd-attn-multi}}(r_{\Theta^*}) - \mathcal{M}_{\text{flash-svd-attn-multi}}(r_{\Theta^*} - 1) \\ &= \mathcal{O}(H (B M + d_{\Theta, h})), \end{aligned}$$

as claimed. \square

Remark 2. *Unless the attention kernel itself is modified to consume low-rank factors directly, compressing activations to rank r_{Θ^*} does not reduce peak memory: one still needs $\mathcal{O}(B H M d_{\Theta, h})$ to materialize Q, K, V for a vanilla kernel.*

Theorem 5 (Multi-Head Compression Threshold). *For a multi-head attention module defined in Definition 1, low-rank compression yields memory savings if and only if*

$$r_{\Theta^*} < \frac{B M \mathcal{D}_{\mathcal{A}}^{\Theta}}{H B M + \mathcal{D}_{\mathcal{A}}^{\Theta}}.$$

The maximum achievable compression ratio, attained in the rank-one case $r_{\Theta^} = 1$, is $\mathcal{O}(\min\{B M, \mathcal{D}_{\mathcal{A}}^{\Theta}/H\})$.*

Proof. From Proposition 2, the off-chip memory required by standard (uncompressed) FlashAttention across all heads is

$$\mathcal{O}(B M \mathcal{D}_{\mathcal{A}}^{\Theta}).$$

In contrast, Theorem 4 shows that under rank- r_{Θ^*} compression, the transient memory for all heads becomes

$$\mathcal{M}_{\text{flash-svd-attn-multi}} = HBMr_{\Theta^*} + r_{\Theta^*}\mathcal{D}_{\mathcal{A}}^{\Theta},$$

which, according to Remark 1, captures only the change-inducing (transient) memory terms.

Memory savings occur when this compressed cost is less than the baseline:

$$HBMr_{\Theta^*} + r_{\Theta^*}\mathcal{D}_{\mathcal{A}}^{\Theta} < BM\mathcal{D}_{\mathcal{A}}^{\Theta}.$$

Solving for r_{Θ^*} yields

$$r_{\Theta^*} < \frac{BM\mathcal{D}_{\mathcal{A}}^{\Theta}}{HBM + \mathcal{D}_{\mathcal{A}}^{\Theta}}.$$

In the extreme low-rank case $r_{\Theta^*} = 1$, the compression ratio becomes

$$\frac{BM\mathcal{D}_{\mathcal{A}}^{\Theta}}{HBM + \mathcal{D}_{\mathcal{A}}^{\Theta}},$$

which scales as $\mathcal{O}(\min\{BM, \mathcal{D}_{\mathcal{A}}^{\Theta}/H\})$, depending on whether the sequence length or head dimension dominates the denominator. \square

Remark 3 (Comparison of Single-Head and Multi-Head Thresholds). *At first glance, Theorem 5 for multi-head attention appears to impose a stricter compression condition than its single-head counterpart (Theorem 3), due to the additional factor of H in the denominator:*

$$r_{\Theta^*}^{(\text{multi})} < \frac{BM\mathcal{D}_{\mathcal{A}}^{\Theta}}{HBM + \mathcal{D}_{\mathcal{A}}^{\Theta}}.$$

However, this threshold is expressed in terms of the per-head rank $r_{\Theta^*}^{(\text{multi})}$, while the single-head condition uses the full attention rank $r_{\Theta^*}^{(\text{single})}$.

In the single-head case, $r_{\Theta^*}^{(\text{single})}$ applies to the full attention dimension $\mathcal{D}_{\mathcal{A}}^{\Theta}$, whereas in the multi-head setting, each head operates on a reduced dimension $d_{\Theta_{\mathcal{A}},h} = \mathcal{D}_{\mathcal{A}}^{\Theta}/H$, and thus its corresponding rank $r_{\Theta^*}^{(\text{multi})}$ is typically much smaller. In fact, they often satisfy the proportional relationship

$$r_{\Theta^*}^{(\text{single})} = \mathcal{O}(H \cdot r_{\Theta^*}^{(\text{multi})}).$$

Substituting this relation into the multi-head threshold recovers the single-head condition:

$$\frac{r_{\Theta^*}^{(\text{single})}}{H} < \frac{BM\mathcal{D}_{\mathcal{A}}^{\Theta}}{HBM + \mathcal{D}_{\mathcal{A}}^{\Theta}} \iff r_{\Theta^*}^{(\text{single})} < \frac{BM\mathcal{D}_{\mathcal{A}}^{\Theta}}{BM + d_{\Theta_{\mathcal{A}},h}},$$

This recovers the single-head threshold exactly (up to constant factors in the $\mathcal{O}(\cdot)$ notation), confirming that the multi-head threshold is in fact more relaxed, since $d_{\Theta_{\mathcal{A}},h} < \mathcal{D}_{\mathcal{A}}^{\Theta}$, making it easier to achieve tangible memory savings through compression.

In practice, multi-head compression often yields superior empirical performance, as it enables head-wise rank customization and offers finer-grained control over compression across different attention subspaces.

We next consider grouped-head compression, where multiple heads are compressed jointly. This PaLU-inspired scheme [1] balances memory savings and model capacity by interpolating between single-head and per-head compression.

Theorem 6 (Grouped-Head Compression Memory Upper Bound). *Consider a multi-head attention module with H heads and total attention dimension $\mathcal{D}_{\mathcal{A}}^{\Theta}$. Grouping the heads into G groups (each of size H/G) and compressing each group's $(BM) \times (\mathcal{D}_{\mathcal{A}}^{\Theta}/G)$ activation to rank r_{Θ^*} yields a total transient off-chip memory of*

$$\begin{aligned}\mathcal{M}_{\text{flash-svd-attn-grouped}} &= O\left(G r_{\Theta^*} \left(BM + \frac{\mathcal{D}_{\mathcal{A}}^{\Theta}}{G}\right)\right) \\ &= O\left(BGM r_{\Theta^*} + r_{\Theta^*} \mathcal{D}_{\mathcal{A}}^{\Theta}\right).\end{aligned}$$

This interpolates between the single-head bound ($G = 1$) and the fully factorized per-head bound ($G = H$), and captures only the change-inducing (transient) memory terms per Remark 1.

Proof. Each group activation has shape $(BM) \times (\mathcal{D}_{\mathcal{A}}^{\Theta}/G)$. A rank- r_{Θ^*} SVD approximation stores

$$(BM + \frac{\mathcal{D}_{\mathcal{A}}^{\Theta}}{G}) \cdot r_{\Theta^*}$$

entries per group. Multiplying by G groups gives the total

$$G r_{\Theta^*} (BM + \frac{\mathcal{D}_{\mathcal{A}}^{\Theta}}{G}) = BGM r_{\Theta^*} + r_{\Theta^*} \mathcal{D}_{\mathcal{A}}^{\Theta},$$

as claimed. \square

Theorem 7 (Marginal Memory Gain from Rank Reduction). *Reducing the rank of each grouped head from r_{Θ^*} to $r_{\Theta^*} - 1$ decreases the total off-chip memory usage by*

$$\begin{aligned}\Delta \mathcal{M}_{\text{flash-svd-attn-grouped}} &= O\left(G \left(BM + \frac{\mathcal{D}_{\mathcal{A}}^{\Theta}}{G}\right)\right) \\ &= O\left(BGM + \mathcal{D}_{\mathcal{A}}^{\Theta}\right).\end{aligned}$$

This quantifies the sensitivity of grouped compression to rank selection and highlights its linear dependency on batch size and number of groups.

Proof. From Theorem 6, grouped compression with rank r_{Θ^*} uses memory

$$G r_{\Theta^*} (BM + \frac{\mathcal{D}_{\mathcal{A}}^{\Theta}}{G}).$$

Replacing r_{Θ^*} with $r_{\Theta^*} - 1$ results in

$$G (r_{\Theta^*} - 1) (BM + \frac{\mathcal{D}_{\mathcal{A}}^{\Theta}}{G}).$$

The difference between the two is

$$G (BM + \frac{\mathcal{D}_{\mathcal{A}}^{\Theta}}{G}) = BGM + \mathcal{D}_{\mathcal{A}}^{\Theta},$$

which establishes the result. \square

Proposition 6 (Grouped-Head Compression Trade-off). *Grouping H heads into G groups (each of size H/G) and applying rank- r_{Θ^*} SVD per group on activations of size $(BM) \times (\mathcal{D}_{\mathcal{A}}^{\Theta}/G)$ reduces off-chip storage from $O(BHM d_{\mathcal{A},h})$ to*

$$O\left(G r_{\Theta^*} (BM + \frac{\mathcal{D}_{\mathcal{A}}^{\Theta}}{G})\right) = O\left(r_{\Theta^*} \mathcal{D}_{\mathcal{A}}^{\Theta} + BGr_{\Theta^*} M\right).$$

This interpolates between the single-head bound ($G = 1$) and the full per-head bound ($G = H$). Moreover, decreasing each group's rank from r_{Θ^} to $r_{\Theta^*} - 1$ yields an additional DRAM saving of*

$$\Delta \mathcal{M}_{\text{group-attn}} = G (BM + \frac{\mathcal{D}_{\mathcal{A}}^{\Theta}}{G}) = BGM + \mathcal{D}_{\mathcal{A}}^{\Theta}.$$

Proof. Each of the G group activations has nominal size $(BM) \times (\mathcal{D}_{\mathcal{A}}^{\Theta}/G)$. By Theorem 2, compressing one group to rank r_{Θ^*} requires $(BM + \frac{\mathcal{D}_{\mathcal{A}}^{\Theta}}{G}) r_{\Theta^*}$ elements of DRAM, and there are G independent groups. Hence the total storage is

$$G (BM + \frac{\mathcal{D}_{\mathcal{A}}^{\Theta}}{G}) r_{\Theta^*} = G r_{\Theta^*} (BM + \frac{\mathcal{D}_{\mathcal{A}}^{\Theta}}{G}).$$

Subtracting the cost at rank $r_{\Theta^*} - 1$ from that at r_{Θ^*} gives $G (BM + \frac{\mathcal{D}_{\mathcal{A}}^{\Theta}}{G})$, establishing the marginal saving in rank reduction. \square

Feed-Forward Network Each Transformer block contains a two-layer, position-wise feed-forward network (FFN) with weight matrices $W_i \in \mathbb{R}^{\mathcal{D}_{\mathcal{A}}^{\Theta} \times \mathcal{D}_{\mathcal{F}}^{\Theta}}$ and $W_o \in \mathbb{R}^{\mathcal{D}_{\mathcal{F}}^{\Theta} \times \mathcal{D}_{\mathcal{A}}^{\Theta}}$. Applied to an input $X \in \mathbb{R}^{B \times M \times \mathcal{D}_{\mathcal{A}}^{\Theta}}$, the intermediate activation $Y = XW_i \in \mathbb{R}^{(BM) \times \mathcal{D}_{\mathcal{F}}^{\Theta}}$ often dominates the per-layer DRAM footprint whenever $\mathcal{D}_{\mathcal{F}}^{\Theta} \gg \mathcal{D}_{\mathcal{A}}^{\Theta}$ (e.g., $\mathcal{D}_{\mathcal{F}}^{\Theta} = 4 \mathcal{D}_{\mathcal{A}}^{\Theta}$ [5, 17, 24, 32]). In what follows, we derive matching upper and lower bounds on the off-chip memory cost of SVD-based compression applied to Y .

Definition 2 (FFN Activation Approximation). *Let $X \in \mathbb{R}^{B \times M \times \mathcal{D}_{\mathcal{A}}^{\Theta}}$ be the input to a two-layer FFN with weight matrices $W_i \in \mathbb{R}^{\mathcal{D}_{\mathcal{A}}^{\Theta} \times \mathcal{D}_{\mathcal{F}}^{\Theta}}$ and $W_o \in \mathbb{R}^{\mathcal{D}_{\mathcal{F}}^{\Theta} \times \mathcal{D}_{\mathcal{A}}^{\Theta}}$, and let $\phi(\cdot)$ be a pointwise nonlinearity. Define the intermediate activation $Y = XW_i \in \mathbb{R}^{(BM) \times \mathcal{D}_{\mathcal{F}}^{\Theta}}$, so that the FFN output is $Z = \phi(Y)W_o$. We say Y admits a rank- r SVD approximation if*

$$\begin{aligned} Y^{[r_{\Theta^*}]} &= U_Y \Sigma_Y V_Y^{\top}, \\ U_Y \in \mathbb{R}^{(BM) \times r_{\Theta^*}}, \quad \Sigma_Y \in \mathbb{R}^{r_{\Theta^*} \times r_{\Theta^*}}, \quad V_Y \in \mathbb{R}^{\mathcal{D}_{\mathcal{F}}^{\Theta} \times r_{\Theta^*}}. \end{aligned} \tag{S2}$$

Theorem 8 (Vanilla SVD FFN Compression Yields No Memory Savings). *Let the feedforward activation matrix $Y \in \mathbb{R}^{(BM) \times \mathcal{D}_{\mathcal{F}}^{\Theta}}$ be defined as in Definition 2, and suppose a standard (non-streaming) rank- r_{Θ^*} SVD is applied to approximate $Y \approx UV^{\top}$, where $U \in \mathbb{R}^{(BM) \times r_{\Theta^*}}$, $V \in \mathbb{R}^{\mathcal{D}_{\mathcal{F}}^{\Theta} \times r_{\Theta^*}}$. Then, the off-chip memory required to store the intermediate activations remains*

$$\mathcal{M}_{\text{naive-svd-ffn}} = O(BM \mathcal{D}_{\mathcal{F}}^{\Theta}),$$

matching the dense baseline $\mathcal{M}_{\text{dense-ffn}}$, and thus yielding no memory savings.

Proof. In the dense FFN case, the output of the intermediate GELU activation $Y \in \mathbb{R}^{(BM) \times \mathcal{D}_{\mathcal{F}}^{\Theta}}$ must be materialized in memory to support the second linear projection.

If we instead apply naive SVD compression to approximate $Y \approx UV^{\top}$, the computation still requires constructing the full matrix Y before performing its factorization, as standard SVD operates on the complete matrix and has no streaming or tiled structure. Thus, the full activation matrix Y must still be loaded into memory in its entirety prior to any compression.

Furthermore, even if the matrix is overwritten post-factorization by its lower-rank factors U and V , this does not avoid the initial memory cost incurred by holding Y . Therefore, the peak transient off-chip memory remains at

$$O(BM \mathcal{D}_{\mathcal{F}}^{\Theta}),$$

as in the dense case.

Hence, in the absence of streaming or blocking techniques, naive FFN compression yields no memory advantage over the dense baseline. \square

FlashSVDFFN V1 and V2: Rank-Aware Streaming FFN Variants. We present two streaming-friendly FFN variants that apply low-rank factorization while balancing compute efficiency and memory usage. We analyze the off-chip memory complexity by focusing only on the *variable* portion stored in HBM, following the scope defined in remark 1.

FlashSVDFFN V1 (algorithm 2) maintains a competitive speed by computing the intermediate projection $P = XU_i \in \mathbb{R}^{(BM) \times r_{\Theta^*}}$ using GEMM. This projection is then streamed tile-by-tile along with SVD factors $V_i^{(d)}, U_o^{(d)}, b_i^{(d)}$, and accumulated into output tiles $Z_{\text{tile}} \in \mathbb{R}^{B \times BM \times r_{\Theta^*}}$. While this avoids full materialization of the FFN output of size $BM \times \mathcal{D}_{\mathcal{F}}^{\Theta}$, it introduces transient memory traffic of size $\mathcal{O}(BMr_{\Theta^*})$, yielding an off-chip footprint of $\mathcal{M}_{\text{flash-svd-ffn-v1}} = \mathcal{O}(BMr_{\Theta^*})$ (theorem 9).

FlashSVDFFN V2 (algorithm S1) eliminates this memory cost entirely by fusing projection and output logic per tile. It streams rows of X and corresponding factor slices on-the-fly, avoiding the explicit construction of P and achieving $\mathcal{M}_{\text{flash-svd-ffn-v2}} = 0$ (theorem 10).

Both variants exhibit distinct advantages: V1 enables fast batched GEMM at the expense of small transient storage, while V2 achieves full off-chip elimination via streaming-aware execution.

Theorem 9 (Partial Memory Reduction via Tiled Factor Streaming in FlashSVDFFN V1). *Algorithm 2 avoids materializing the full activation $Y \in \mathbb{R}^{BM \times \mathcal{D}_{\mathcal{F}}^{\Theta}}$ by streaming over the intermediate width d in tiles of size $B_{\mathcal{D}_{\mathcal{F}}}^{\Theta}$. Consequently, the peak off-chip memory required for intermediate activations satisfies*

$$\mathcal{M}_{\text{flash-svd-ffn-v1}} = \mathcal{O}(BMr_{\Theta^*}).$$

Proof. At each iteration over $d = 0, \dots, \mathcal{D}_{\mathcal{F}}^{\Theta}$, Algorithm 2 loads a tile of SVD factors $V_i^{(d)} \in \mathbb{R}^{r_{\Theta^*} \times B_{\mathcal{D}_{\mathcal{F}}}^{\Theta}}$, $U_o^{(d)} \in \mathbb{R}^{B_{\mathcal{D}_{\mathcal{F}}}^{\Theta} \times r_{\Theta^*}}$, and bias $b_i^{(d)} \in \mathbb{R}^{B_{\mathcal{D}_{\mathcal{F}}}^{\Theta}}$. It then immediately computes the corresponding intermediate slice $Y^{(d)} = \phi(PV_i^{(d)} + b_i^{(d)})$ and its projection $Y^{(d)}U_o^{(d)}$, which are accumulated into the on-chip buffer Z_{tile} . Since $Y^{(d)}$ is constructed and consumed on-the-fly, and never fully materialized, the memory footprint is limited to storing $P \in \mathbb{R}^{BM \times r_{\Theta^*}}$ and $Z_{\text{tile}} \in \mathbb{R}^{BM \times r_{\Theta^*}}$. Therefore, the total intermediate off-chip memory used is

$$\mathcal{M}_{\text{flash-svd-ffn-v1}} = \mathcal{O}(BMr_{\Theta^*}),$$

which is much smaller than the dense baseline $\mathcal{O}(BMD_{\mathcal{F}}^{\Theta})$, but still nonzero. \square

Theorem 10 (Memory-Free FFN Streaming via Fully Fused Tiling). *Algorithm S1 executes the entire FFN forward pass without materializing any intermediate tensor in off-chip memory. Specifically, the peak off-chip memory used for intermediate FFN activations satisfies*

$$\mathcal{M}_{\text{flash-svd-ffn-v2}} = 0.$$

Proof. Algorithm S1 eliminates the need to store $P = XU_i$ in off-chip memory by recomputing each component $P_{\text{tile}}[:, :, k] \leftarrow X[:, \ell : \ell + BM, :] \cdot U_i[:, k]$ on-the-fly for $k = 0, \dots, r_{\Theta^*} - 1$. For each block over $d = 0, \dots, \mathcal{D}_{\mathcal{F}}^{\Theta}$, it incrementally constructs the partial activation tensor $Y \in \mathbb{R}^{B \times BM \times B_{\mathcal{D}_{\mathcal{F}}}^{\Theta}}$ via

$$Y += P_{\text{tile}}[:, :, k] \cdot V_i[k, d : d + B_{\mathcal{D}_{\mathcal{F}}}^{\Theta}],$$

followed by fused activation and projection

$$Z_{\text{tile}} += \phi \left(Y + b_i[d : d + B_{\mathcal{D}_{\mathcal{F}}}^{\Theta}] \right) \cdot U_o[d : d + B_{\mathcal{D}_{\mathcal{F}}}^{\Theta}, k].$$

Since all computation and accumulation are performed in on-chip SRAM and no intermediate tensor is written to \mathcal{M} , the memory footprint is limited to streaming only the SVD weights and biases. The final output is computed as $O = Z_{\text{tile}}V_o + b_o$ in a single post-processing step.

The fused implementation performs the same number of floating-point operations as V1:

$$\text{FLOPs} = O\left(BMr_{\Theta^*}D_{\mathcal{F}}^{\Theta} + BMr_{\Theta^*}D_{\mathcal{A}}^{\Theta}\right),$$

but with strictly lower memory traffic (more details analysis for FLOPS can be found in Theorem 14). Therefore, it achieves

$$\mathcal{M}_{\text{flash-svd-ffn-V2}} = 0 \quad \text{vs.} \quad \mathcal{M}_{\text{flash-svd-ffn-V1}} = O(BMr_{\Theta}^*),$$

while maintaining equal arithmetic complexity. \square

Compression Trade-offs between Attention and FFN. A common misconception is that compressing attention alone—via FlashAttention [2]—suffices for end-to-end memory savings. However, this neglects the downstream footprint of the feed-forward network (FFN). In fact, aggressively compressing only attention can shift the memory bottleneck to the FFN, motivating the need to compress both components. The following result formalizes this balance.

Theorem 11 (FFN Bottleneck under Attention-Only Compression). *In standard transformer architectures with $\mathcal{D}_{\mathcal{F}}^{\Theta} \geq 4\mathcal{D}_{\mathcal{A}}^{\Theta}$, compressing attention alone (with rank $r_{\Theta^*} \ll \mathcal{D}_{\mathcal{A}}^{\Theta}$) results in the FFN layer dominating off-chip memory usage.*

Proof. By Theorem 2, the memory footprint of SVD-compressed attention is

$$\mathcal{M}_{\text{flash-svd-attn}} = O(r_{\Theta^*}(BM + \mathcal{D}_{\mathcal{A}}^{\Theta})),$$

while the dense FFN incurs

$$\mathcal{M}_{\text{dense-ffn}} = O(BM\mathcal{D}_{\mathcal{F}}^{\Theta}).$$

For typical models such as BERT, RoBERTa, LLaMA, and OPT [5, 17, 24, 32], we have $\mathcal{D}_{\mathcal{F}}^{\Theta} = 4\mathcal{D}_{\mathcal{A}}^{\Theta}$. Then:

$$\frac{\mathcal{M}_{\text{dense-ffn}}}{\mathcal{M}_{\text{flash-svd-attn}}} = \frac{BM \cdot 4\mathcal{D}_{\mathcal{A}}^{\Theta}}{r_{\Theta^*}(BM + \mathcal{D}_{\mathcal{A}}^{\Theta})} = \frac{1}{\frac{r_{\Theta^*}}{4\mathcal{D}_{\mathcal{A}}^{\Theta}} + \frac{r_{\Theta^*}}{BM}} \gg 1,$$

since both $\frac{r_{\Theta^*}}{4\mathcal{D}_{\mathcal{A}}^{\Theta}} \ll 1$ and $\frac{r_{\Theta^*}}{BM} \ll 1$ hold in typical settings where $r_{\Theta^*} \ll \mathcal{D}_{\mathcal{A}}^{\Theta}$ and $r_{\Theta^*} \ll BM$. Thus, the FFN dominates off-chip usage. \square

This result motivates the design of rank-aware FFN compression, ensuring neither component becomes a performance bottleneck.

Proposition 7 (Per-Rank Sensitivity of FFN Memory). *Let the FlashSVDFFN memory cost at rank r_{Θ^*} be*

$$\mathcal{M}_{\text{flash-svd-ffn-V1}}(r_{\Theta^*}) = O(r_{\Theta^*}(BM + \mathcal{D}_{\mathcal{F}}^{\Theta})).$$

Then the reduction in off-chip memory for decreasing the rank by 1 is

$$\Delta\mathcal{M}_{\text{flash-svd-ffn-V1}} = O(\mathcal{D}_{\mathcal{F}}^{\Theta}),$$

independent of r_{Θ^} .*

Proof. We have

$$\begin{aligned}
 \Delta \mathcal{M}_{\text{flash-svd-ffn-V1}} &= \mathcal{M}_{\text{ffn-V1}}(r_{\Theta^*}) - \mathcal{M}_{\text{ffn-V1}}(r_{\Theta^*} - 1) \\
 &= r_{\Theta^*} (BM + \mathcal{D}_{\mathcal{F}}^{\Theta}) \\
 &\quad - (r_{\Theta^*} - 1)(BM + \mathcal{D}_{\mathcal{F}}^{\Theta}) \\
 &= (BM + \mathcal{D}_{\mathcal{F}}^{\Theta}) \in O(BM + \mathcal{D}_{\mathcal{F}}^{\Theta}).
 \end{aligned}$$

□

Proposition 8 (Per-Rank Sensitivity of FFN Memory in FlashSVDFFN-V2). *Let the FlashSVDFFN-V2 memory cost at rank r_{Θ^*} be*

$$\mathcal{M}_{\text{flash-svd-ffn-V2}}(r_{\Theta^*}) = O(r_{\Theta^*} \cdot \mathcal{D}_{\mathcal{F}}^{\Theta}),$$

which removes the dependence on BM via full streaming. Then the per-rank reduction is

$$\Delta \mathcal{M}_{\text{flash-svd-ffn-V2}} = O(\mathcal{D}_{\mathcal{F}}^{\Theta}), \quad (\text{S3})$$

independent of r_{Θ^} and BM .*

Proof. We again compute the difference:

$$\begin{aligned}
 \Delta \mathcal{M}_{\text{flash-svd-ffn-V2}} &= \mathcal{M}_{\text{ffn-V2}}(r_{\Theta^*}) - \mathcal{M}_{\text{ffn-V2}}(r_{\Theta^*} - 1) \\
 &= r_{\Theta^*} \cdot \mathcal{D}_{\mathcal{F}}^{\Theta} - (r_{\Theta^*} - 1) \cdot \mathcal{D}_{\mathcal{F}}^{\Theta} \\
 &= \mathcal{D}_{\mathcal{F}}^{\Theta} \in O(\mathcal{D}_{\mathcal{F}}^{\Theta}).
 \end{aligned}$$

□

Theorem 12 (Relative Memory Reduction of FFN under Low-Rank Compression). *Let the dense FFN memory usage be*

$$\mathcal{M}_{\text{dense-ffn}} = O(BM \mathcal{D}_{\mathcal{F}}^{\Theta}),$$

and the FlashSVD-compressed usage at rank r_{Θ^} be*

$$\mathcal{M}_{\text{flash-svd-ffn}} = O(r_{\Theta^*}(BM + \mathcal{D}_{\mathcal{F}}^{\Theta})).$$

Then the memory ratio satisfies

$$\frac{\mathcal{M}_{\text{flash-svd-ffn}}}{\mathcal{M}_{\text{dense-ffn}}} = \frac{r_{\Theta^*}}{\mathcal{D}_{\mathcal{F}}^{\Theta}} + O\left(\frac{r_{\Theta^*}}{BM}\right).$$

Proof. Compute the ratio:

$$\begin{aligned}
 \frac{\mathcal{M}_{\text{flash-svd-ffn}}}{\mathcal{M}_{\text{dense-ffn}}} &= \frac{r_{\Theta^*}(BM + \mathcal{D}_{\mathcal{F}}^{\Theta})}{BM \mathcal{D}_{\mathcal{F}}^{\Theta}} \\
 &= \frac{r_{\Theta^*}}{\mathcal{D}_{\mathcal{F}}^{\Theta}} \left(1 + \frac{\mathcal{D}_{\mathcal{F}}^{\Theta}}{BM}\right) \\
 &= \frac{r_{\Theta^*}}{\mathcal{D}_{\mathcal{F}}^{\Theta}} + O\left(\frac{r_{\Theta^*}}{BM}\right),
 \end{aligned}$$

where the second term vanishes as $BM \rightarrow \infty$.

□

Theorem 13 (Combined FlashSVD Memory Bound). *Compressing both multi-head attention and FFN using FlashSVD with rank r_{Θ^*} , the total per-layer off-chip memory is bounded by*

$$\mathcal{M}_{\text{flash-svd-total}} = O(r_{\Theta^*}(BM + \mathcal{D}_{\mathcal{A}}^{\Theta} + \mathcal{D}_{\mathcal{F}}^{\Theta})),$$

assuming FFN follows the V1 layout (with activations of shape $(B, M, \mathcal{D}_{\mathcal{F}}^{\Theta})$). This bound also dominates the cost for the V2 layout, since V1 includes the intermediate activations from both input and output projections.

Proof. By Proposition 7, FlashSVD compression of the FFN (V1 variant) requires

$$\mathcal{M}_{\text{flash-svd-fnn}} = O(r_{\Theta^*}(BM + \mathcal{D}_{\mathcal{F}}^{\Theta})),$$

and attention requires

$$\mathcal{M}_{\text{flash-svd-attn}} = O(r_{\Theta^*}(BM + \mathcal{D}_{\mathcal{A}}^{\Theta})),$$

so their sum satisfies

$$\begin{aligned} \mathcal{M}_{\text{flash-svd-total}} &= O(r_{\Theta^*}(2BM + \mathcal{D}_{\mathcal{A}}^{\Theta} + \mathcal{D}_{\mathcal{F}}^{\Theta})) \\ &= O(r_{\Theta^*}(BM + \mathcal{D}_{\mathcal{A}}^{\Theta} + \mathcal{D}_{\mathcal{F}}^{\Theta})). \end{aligned}$$

In practice, the FFN width dominates over attention ($\mathcal{D}_{\mathcal{F}}^{\Theta} \gg \mathcal{D}_{\mathcal{A}}^{\Theta}$), so total memory scales primarily with $r_{\Theta^*} \cdot \mathcal{D}_{\mathcal{F}}^{\Theta}$ and $r_{\Theta^*} \cdot BM$. Thus, total resource usage is jointly governed by sequence length and chosen compression rank. This further confirms Theorem 11: to achieve balanced memory reduction across all components, one must incorporate FFN-specific strategies—such as FlashSVDFFN proposed in our work—beyond uniform low-rank compression alone.

Since V1 includes all intermediate FFN activations, this result also upper bounds the memory of V2. \square

Decoder Memory Cost Analysis The decoder inference proceeds in two distinct phases—*prefill* and *decoding*—each exhibiting different peak-memory behaviors. To avoid re-computing all past keys and values at every step, we employ a KV-cache: once a key–value pair is produced, it is retained on-chip (or in HBM) for all subsequent steps.

Prefill Phase During prefill, we process the entire input sequence of length M in one shot. At each of the ℓ -th decoder layers, the hidden state

$$X_{\text{prefill}} \in \mathbb{R}^{B \times M \times \mathcal{D}_{\mathcal{A}}^{\Theta}}$$

is projected to low-rank queries, keys, and values:

$$P_q, P_k, P_v \in \mathbb{R}^{B \times M \times r_{\Theta^*}}.$$

We then compute

$$A = \text{softmax}\left(\frac{QK^{\top}}{d_h}\right),$$

but rather than materializing the full BHM^2 attention matrix and dense Q, K, V factors, a streaming attention kernel (e.g. FlashSVDAttn) only allocates $O(BM r_{\Theta^*})$ buffer at any time. Meanwhile, the KV-cache permanently stores the keys and values for all M positions, requiring $2\ell BM r_{\Theta^*}$ elements of memory (for keys and values). Thus, the *prefill* peak memory is dominated by the sum of:

- Two large FFN GEMMs per layer (as in the encoder), each with peak memory $O(BM r_{\Theta^*} + r_{\Theta^*} \mathcal{D}_{\mathcal{A}}^{\Theta})$ if FlashSVDFFN is applied.
- The KV-cache cost $2\ell BM r_{\Theta^*}$.

Decoding Phase Once prefill is complete, each new token is generated one at a time. At step t , we compute a single new query

$$q_t \in \mathbb{R}^{B \times 1 \times r_{\Theta^*}}$$

and attend against the cached keys $K_{\leq t-1} \in \mathbb{R}^{B \times (t-1) \times r_{\Theta^*}}$ and values $V_{\leq t-1}$ through the causal mask. The streaming attention now needs buffers of size $O(B(t-1)r_{\Theta^*})$ for the dot-products and softmax, plus space for the new key and value. Since t grows from 1 to M , the worst-case buffer remains $O(BMr_{\Theta^*})$, but this never exceeds the prefill cache. The subsequent FFN uses the same rank-aware fusion (FlashSVDFFN) with peak memory $O(Br_{\Theta^*} + r_{\Theta^*}\mathcal{D}_{\mathcal{A}}^{\Theta})$.

Overall Bound By (i) streaming attention over low-rank projections and (ii) fusing the FFN, the decoder’s peak-memory across both phases is bounded by

$$O(LBMr_{\Theta^*} + (Br_{\Theta^*} + r_{\Theta^*}\mathcal{D}_{\mathcal{A}}^{\Theta})),$$

ensuring that neither sequence length nor model width blows up the memory footprint beyond linear dependence on the chosen low rank.

S2.4. Computation Complexity Analysis

In this section, we quantify how rank- r SVD compression reduces compute and end-to-end kernel latency. We begin with idealized FLOP-count bounds, then incorporate I/O and memory-bandwidth effects, and finally analyze the trade-offs introduced by reconstruction overhead in both attention and FFN blocks.

FLOP-Count Reduction

Theorem 14 (Pure FLOP-Count Speedup). *Let a Transformer layer with hidden dimension $\mathcal{D}_{\mathcal{A}}^{\Theta}$, FFN hidden size $\mathcal{D}_{\mathcal{F}}^{\Theta}$, sequence length M , and batch size B require*

$$O((\mathcal{D}_{\mathcal{A}}^{\Theta})^2 MB + \mathcal{D}_{\mathcal{A}}^{\Theta} \mathcal{D}_{\mathcal{F}}^{\Theta} MB)$$

FLOPs in the full-rank case. If all self-attention activations and FFN intermediates are compressed to rank r_{Θ^} , the FLOP count becomes*

$$O(r_{\Theta^*} \mathcal{D}_{\mathcal{A}}^{\Theta} MB + r_{\Theta^*}^2 MB + r_{\Theta^*} \mathcal{D}_{\mathcal{F}}^{\Theta} MB).$$

Thus, the asymptotic speedup factor is

$$\Theta\left(\frac{\mathcal{D}_{\mathcal{A}}^{\Theta} + \mathcal{D}_{\mathcal{F}}^{\Theta}}{r_{\Theta^*} + \frac{r_{\Theta^*}^2}{\mathcal{D}_{\mathcal{A}}^{\Theta}}}\right).$$

In particular, when $r_{\Theta^} \ll \min\{\mathcal{D}_{\mathcal{A}}^{\Theta}, \mathcal{D}_{\mathcal{F}}^{\Theta}\}$, the numerator dominates and the speedup is significant.*

Proof. In the full-rank Transformer layer, computing self-attention requires forming the QK^T and SV , for $S = \text{Softmax}(\frac{QK^T}{d_{\Theta_{\mathcal{A}},h}})$ products at cost $O((\mathcal{D}_{\mathcal{A}}^{\Theta})^2 MB)$, and the two-layer FFN costs $O(\mathcal{D}_{\mathcal{A}}^{\Theta} \mathcal{D}_{\mathcal{F}}^{\Theta} MB)$, for a total of $O((\mathcal{D}_{\mathcal{A}}^{\Theta})^2 MB + \mathcal{D}_{\mathcal{A}}^{\Theta} \mathcal{D}_{\mathcal{F}}^{\Theta} MB)$.

When all attention activations and FFN intermediates admit rank- r approximations, each matrix–matrix multiply involving a $\mathcal{D}_{\mathcal{A}}^{\Theta} \times \mathcal{D}_{\mathcal{A}}^{\Theta}$ or $\mathcal{D}_{\mathcal{A}}^{\Theta} \times \mathcal{D}_{\mathcal{F}}^{\Theta}$ block is replaced by a sequence of three multiplies of shapes

$\mathcal{D}_{\mathcal{A}}^{\Theta} \times r_{\Theta^*}$, $r_{\Theta^*} \times r_{\Theta^*}$, and $r_{\Theta^*} \times \mathcal{D}_{\mathcal{A}}^{\Theta}$ (or $r_{\Theta^*} \times \mathcal{D}_{\mathcal{F}}^{\Theta}$), yielding $O(r_{\Theta^*} \mathcal{D}_{\mathcal{A}}^{\Theta} M B + r_{\Theta^*}^2 M B + r_{\Theta^*} \mathcal{D}_{\mathcal{F}}^{\Theta} M B)$ total FLOPs.

Comparing these two expressions, when $r_{\Theta^*} \ll \mathcal{D}_{\mathcal{A}}^{\Theta}, \mathcal{D}_{\mathcal{F}}^{\Theta}$ the dominant terms yield an asymptotic speedup factor

$$\frac{\left(\mathcal{D}_{\mathcal{A}}^{\Theta}\right)^2 + \mathcal{D}_{\mathcal{A}}^{\Theta} \mathcal{D}_{\mathcal{F}}^{\Theta}}{r_{\Theta^*} \mathcal{D}_{\mathcal{A}}^{\Theta} + r_{\Theta^*}^2 + r_{\Theta^*} \mathcal{D}_{\mathcal{F}}^{\Theta}} = \Theta\left(\frac{\mathcal{D}_{\mathcal{A}}^{\Theta} + \mathcal{D}_{\mathcal{F}}^{\Theta}}{r_{\Theta^*} + \frac{r_{\Theta^*}^2}{\mathcal{D}_{\mathcal{A}}^{\Theta}}}\right).$$

This confirms the claimed efficiency gain of the low-rank approximation. \square

Latency with I/O and Bandwidth

Theorem 15 (Bandwidth-Bounded Latency). *Assume a GPU memory bandwidth of β (bytes/s) and that each activation element is 4 bytes. Then the end-to-end latency T per layer is lower-bounded by*

$$T \geq \max\left\{\frac{\text{FLOPs}}{\text{PeakFLOP/s}}, \frac{4 N_{\text{bytes}}}{\beta}\right\},$$

where $N_{\text{bytes}} = O(BM(\mathcal{D}_{\mathcal{A}}^{\Theta} + \mathcal{D}_{\mathcal{F}}^{\Theta}))$ in the full-rank case and $O(MBr_{\Theta^*} + r_{\Theta^*}\mathcal{D}_{\mathcal{A}}^{\Theta} + r_{\Theta^*}\mathcal{D}_{\mathcal{F}}^{\Theta})$ under rank- r compression.

Proof. We invoke the standard roofline argument, which lower-bounds end-to-end latency by the worse of compute-bound and I/O-bound costs.

Compute bound. Let FLOPs be the total floating-point operations performed in one layer, and PeakFLOP/s be the device's maximum sustained FLOP rate. Then even if all compute units are perfectly utilized, the time cannot be smaller than

$$\frac{\text{FLOPs}}{\text{PeakFLOP/s}}.$$

Bandwidth bound. Similarly, suppose we must read and/or write N_{bytes} bytes of activation data (each element 4 byte) between DRAM and on-chip buffers. With peak bandwidth β bytes/s, the I/O time is at least $\frac{N_{\text{bytes}}}{\beta}$. Accounting explicitly for the 4 byte per element gives the form $\frac{4N_{\text{elements}}}{\beta}$, which we absorb into the notation above.

Data-movement volumes. In the full-rank case, we must transfer all query/key/value and FFN activations of total size $N_{\text{bytes_in}} = 4(3BM\mathcal{D}_{\mathcal{A}}^{\Theta} + 2BM\mathcal{D}_{\mathcal{F}}^{\Theta}) = O(BM(\mathcal{D}_{\mathcal{A}}^{\Theta} + \mathcal{D}_{\mathcal{F}}^{\Theta}))$ up to the SRAM. In case of writing, the memory is bounded by $N_{\text{bytes_out}} = 2BMD_{\mathcal{A}}^{\Theta} = O(BMD_{\mathcal{A}}^{\Theta})$. Under rank- r_{Θ^*} compression, only the low-rank factors are moved:

$$\begin{aligned} N_{\text{bytes_in}} &= 4(4BMr_{\Theta^*} + 3r_{\Theta^*}\mathcal{D}_{\mathcal{A}}^{\Theta} + 2r_{\Theta^*}\mathcal{D}_{\mathcal{F}}^{\Theta}) \\ &= O(MBr_{\Theta^*} + r_{\Theta^*}\mathcal{D}_{\mathcal{A}}^{\Theta} + r_{\Theta^*}\mathcal{D}_{\mathcal{F}}^{\Theta}). \end{aligned} \tag{S4}$$

and the $N_{\text{bytes_out}}$ remains the same.

Combining the compute-bound and bandwidth-bound terms yields the desired lower bound

$$T \geq \max\left\{\frac{\text{FLOPs}}{\text{PeakFLOP/s}}, \frac{4 N_{\text{bytes_in}} + N_{\text{bytes_out}}}{\beta}\right\}.$$

\square

Table S2: Computation-efficiency ablation: $B=16$, varying context length M , FFN ranks. Shown are **Time (ms)** and **Speedup** vs. Dense.

Version	Rank	Mild Contexts ($M \leq 256$)				Long Contexts ($M \geq 512$)			
		M=128		M=256		M=512		M=1024	
		Time	Speedup	Time	Speedup	Time	Speedup	Time	Speedup
Dense	Full	0.14	1.00×	0.29	1.00×	0.68	1.00×	1.47	1.00×
FlashSVDFFN V1	768	2.13	0.07×	4.05	0.07×	8.30	0.08×	16.77	0.09×
	384	0.68	0.21×	1.26	0.23×	2.46	0.28×	4.99	0.30×
	192	0.27	0.53×	0.54	0.53×	0.86	0.79×	1.82	0.81×
	96	0.19	0.74×	0.23	1.26×	1.67	1.60×	0.78	1.88×
	768	3.45	0.04×	7.05	0.04×	13.43	0.05×	27.10	0.05×
FlashSVDFFN V2	384	1.82	0.08×	3.89	0.07×	7.16	0.09×	14.42	0.10×
	192	1.14	0.12×	2.14	0.13×	4.20	0.16×	8.30	0.18×
	96	0.75	0.19×	1.39	0.21×	10.64	0.25×	5.33	0.28×

For milder contexts ($M = 128, 256$), FlashSVDFFN V1 at low ranks already approaches or exceeds Dense throughput; for long contexts ($M \geq 512$), the kernel becomes compute-bound and speedups diminish.

Table S3: FlashSVD Attention Ablation ($B=16$): time and speedup vs. Dense at mild vs. long contexts.

Rank	Mild Contexts ($M \leq 256$)				Long Contexts ($M \geq 512$)			
	M=128		M=256		M=512		M=1024	
	Time (ms)	Speedup	Time (ms)	Speedup	Time (ms)	Speedup	Time (ms)	Speedup
Dense	0.38	1.00×	0.74	1.00×	2.31	1.00×	6.98	1.00×
64	0.61	0.62×	0.83	0.89×	2.21	1.05×	5.65	1.24×
48	0.61	0.62×	0.81	0.92×	2.10	1.10×	5.41	1.29×
32	0.60	0.62×	0.74	1.00×	1.79	1.29×	4.57	1.53×
16	0.61	0.62×	0.68	1.08×	1.68	1.37×	4.25	1.64×

For moderate contexts ($M = 128, 256$), FlashSVDAttention achieves up to 38% of Dense speed at full rank and even approaches parity at low ranks; at large contexts ($M \geq 512$), it becomes compute-bound, yielding speedups above 1×.

Table S4: Full FlashSVD Attention Rank benchmarking on NVIDIA L40S GPU ($d_{\text{model}} = 768$, $n_{\text{heads}} = 12$, $d_{\text{ff}} = 3072$).

(a) $B = 1$										(b) $B = 16$										(c) $B = 64$									
M	Rank	Time (ms)	Mem (MB)	Err	Params (K)	Speedup $\frac{M}{\text{vs. Dense}}$	Rank	Time (ms)	Mem (MB)	Err	Params (K)	Speedup $\frac{M}{\text{vs. Dense}}$	Rank	Time (ms)	Mem (MB)	Err	Params (K)	Speedup $\frac{M}{\text{vs. Dense}}$											
128	Dense	0.57	26.3	0.0000	2362	1.00×	Dense	0.38	77.7	0.0000	2362	1.00×	Dense	1.43	240.5	0.0000	2362	1.00×											
	64	0.88	41.5	0.0003	2510	0.65×	64	0.61	88.8	0.0003	2510	0.62×	64	1.61	254.8	0.0003	2510	0.89×											
	48	0.86	39.8	0.0204	2031	0.67×128	48	0.61	86.2	0.0210	2031	0.62×128	48	1.57	230.6	0.0208	2031	0.91×											
	32	0.85	39.3	0.0296	1551	0.68×	32	0.60	83.9	0.0305	1551	0.62×	32	1.41	221.7	0.0300	1551	1.02×											
	16	0.84	38.5	0.0381	1072	0.68×	16	0.61	79.6	0.0377	1072	0.62×	16	1.29	211.5	0.0371	1072	1.11×											
256	Dense	0.55	41.7	0.0000	2362	1.00×	Dense	0.74	123.2	0.0000	2362	1.00×	Dense	3.96	378.6	0.0000	2362	1.00×											
	64	0.85	45.0	0.0003	2510	0.65×	64	0.83	139.2	0.0002	2510	0.89×	64	3.56	434.2	0.0002	2510	1.11×											
	48	0.87	43.1	0.0155	2031	0.64×256	48	0.81	135.9	0.0150	2031	0.92×256	48	3.21	425.4	0.0153	2031	1.23×											
	32	0.85	42.2	0.0240	1551	0.65×	32	0.74	130.5	0.0218	1551	1.00×	32	3.00	407.4	0.0220	1551	1.32×											
	16	0.87	40.5	0.0283	1072	0.64×	16	0.68	124.7	0.0270	1072	1.08×	16	2.79	387.7	0.0271	1072	1.42×											
512	Dense	0.57	50.6	0.0000	2362	1.00×	Dense	2.31	298.5	0.0000	2362	1.00×	Dense	10.40	1090.7	0.0000	2362	1.00×											
	64	0.85	50.4	0.0002	2510	0.67×	64	2.21	236.6	0.0002	2510	1.05×	64	8.66	829.2	0.0002	2510	1.20×											
	48	0.62	48.0	0.0104	2031	0.92×512	48	2.10	231.5	0.0113	2031	1.10×512	48	8.31	816.3	0.0112	2031	1.25×											
	32	0.57	46.5	0.0150	1551	1.00×	32	1.79	221.4	0.0162	1551	1.29×	32	7.16	779.4	0.0161	1551	1.45×											
	16	0.57	45.0	0.0185	1072	1.00×	16	1.68	212.1	0.0197	1072	1.37×	16	6.72	742.9	0.0196	1072	1.55×											
1024	Dense	0.37	92.0	0.0000	2362	1.00×	Dense	6.98	946.3	0.0000	2362	1.00×	Dense	29.19	3681.9	0.0000	2362	1.00×											
	64	0.55	65.6	0.0002	2510	0.66×	64	5.65	434.2	0.0002	2510	1.24×	64	23.45	1622.1	0.0002	2510	1.24×											
	48	0.57	62.7	0.0088	2031	0.64×1024	48	5.41	426.0	0.0087	2031	1.29×1024	48	22.46	1595.5	0.0086	2031	1.30×											
	32	0.55	59.6	0.0124	1551	0.66×	32	4.57	407.5	0.0123	1551	1.53×	32	19.35	1523.4	0.0122	1551	1.51×											
	16	0.57	58.5	0.0148	1072	0.65×	16	4.25	389.1	0.0149	1072	1.64×	16	18.61	1449.6	0.0148	1072	1.57×											

Table S5: Full FlashSVDFFN Rank benchmarking on NVIDIA L40S GPU ($d_{\text{model}} = 768$, $d_{\text{ff}} = 3072$).

(a) $B = 1$										(b) $B = 16$										(c) $B = 64$									
M	Version	Rank	Time (ms)	Mem (MB)	Err	Speedup $\frac{M}{\text{vs. Full}}$	Version	Rank	Time (ms)	Mem (MB)	Err	Speedup $\frac{M}{\text{vs. Full}}$	Version	Rank	Time (ms)	Mem (MB)	Err	Speedup $\frac{M}{\text{vs. Full}}$											
128	Dense	Full	0.10	19.4	0.0000	1.00×	Dense	Full	0.14	61.0	0.0000	1.00×	Dense	Full	0.69	186.5	0.0000	1.00×											
	Flash-v1	768	0.35	30.3	0.0008	0.29×	Flash-v1	768	2.13	56.4	0.0008	0.07×	Flash-v1	768	8.28	137.4	0.0008	0.08×											
	Flash-v2	768	1.12	30.4	0.0008	0.09×128	Flash-v2	768	3.45	48.6	0.0008	0.04×128	Flash-v2	768	13.33	101.1	0.0008	0.05×											
	Flash-v1	384	0.27	24.1	0.7148	0.38×	Flash-v1	384	0.68	44.8	0.7101	0.21×	Flash-v1	384	2.56	107.4	0.7114	0.27×											
	Flash-v2	384	0.62	23.8	0.7148	0.17×	Flash-v2	384	1.82	41.0	0.7101	0.08×	Flash-v2	384	7.26	88.9	0.7114	0.09×											
256	Dense	Full	0.11	23.2	0.0000	1.00×	Dense	Full	0.29	85.5	0.0000	1.00×	Dense	Full	1.47	282.5	0.0000	1.00×											
	Flash-v1	768	0.39	32.1	0.0008	0.27×	Flash-v1	768	4.05	75.3	0.0008	0.07×	Flash-v1	768	16.71	208.5	0.0008	0.09×											
	Flash-v2	768	1.11	30.6	0.0008	0.09×256	Flash-v2	768	7.05	65.5	0.0008	0.04×256	Flash-v2	768	27.17	173.9	0.0008	0.05×											
	Flash-v1	384	0.29	26.0	0.7115	0.36×	Flash-v1	384	1.26	65.3	0.7136	0.23×	Flash-v1	384	5.05	191.6	0.7102	0.29×											
	Flash-v2	384	0.62	24.8	0.7115	0.17×	Flash-v2	384	3.89	57.5	0.7136	0.07×	Flash-v2	384	14.45	154.8	0.7103	0.10×											
512	Dense	Full	0.10	27.3	0.0000	1.00×	Dense	Full	0.68	150.5	0.0000	1.00×	Dense	Full	10.40	1090.7	0.0000	1.00×											
	Flash-v1	768	0.61	34.9	0.0008	0.17×	Flash-v1	768	8.30	118.8	0.0008	0.08×	Flash-v1	768	8.66	829.2	0.0002	1.20×											
	Flash-v2	768	1.16	32.9	0.0008	0.09×512	Flash-v2	768	13.43	101.6	0.0008	0.05×512	Flash-v2	768	54.82	317.0	0.0008	0.05×											
	Flash-v1	384	0.27	28.0	0.7133	0.37×	Flash-v1	384	2.46	106.9	0.7105	0.28×	Flash-v1	384	9.91	358.8	0.7090	0.27×											
	Flash-v2	384	0.63	26.9	0.7133	0.16×	Flash-v2	384	7.16	88.8	0.7105	0.09×	Flash-v2	384	29.21	286.8	0.7090	0.09×											
1024	Dense	Full	0.10	35.5	0.0000	1.00×	Dense	Full	1.47	282.5	0.0000	1.00×	Dense	Full	29.19	3681.9	0.0000	1.00×											
	Flash-v1	768	1.12	40.8	0.0008	0.09×	Flash-v1	768	16.77	209.4	0.0008	0.09×	Flash-v1	768	74.28	749.3	0.0008	0.08×											
	Flash-v2	768	2.34	38.6	0.0008	0.04×1024	Flash-v2	768	27.10	173.1	0.0008	0.05×1024	Flash-v2	768	108.50	604.4	0.0008	0.05×											
	Flash-v1	384	0.38	34.5	0.7098	0.26×	Flash-v1	384	4.99	191.4	0.7134	0.30×	Flash-v1	384	21.40	694.8	0.7133	0.27×											
	Flash-v2	384	1.31	32.6	0.7098	0.07×	Flash-v2	384	14.42	154.8	0.7134	0.10×	Flash-v2	384	58.20	550.8	0.7133	0.10×											

Table S6: Finetuned FlashSVD shows Strong Potential in Edge Deployment (batch_size=32)

SST-2				
Rank	Acc (%)	Trans.	Peak	Lat
dense	92.52	143.3	560.9	66.9
32-192	88.30	107.7	330.8	74.4
32-192 (SVD)	88.19	203.7	426.9	88.9
16-96	86.81	105.8	263.9	70.3
16-96 (SVD)	86.81	201.9	359.9	78.7
Unfinetuned SST-2				
Rank	Acc (%)	Trans.	Peak	Lat
32-192	58.82	110.1	328.6	92.7
32-192 (SVD)	58.82	206.1	424.6	131.4
16-96	50.89	109.1	265.2	94.7
16-96 (SVD)	50.89	205.1	361.2	124.9
STS-B (pearson accuracy)				
Rank	Acc (%)	Trans.	Peak	Lat
dense	81.41	281.3	699.0	98.8
32-192	71.49	206.3	429.4	112.5
32-192 (SVD)	71.49	398.3	621.5	118.0
40-240	80.52	207.8	460.8	114.8
40-240 (SVD)	80.52	399.8	652.8	128.9
Unfinetuned STS-B				
Rank	Acc (%)	Trans.	Peak	Lat
32-192	0.76	215.2	433.7	126.0
32-192 (SVD)	0.78	407.1	625.7	137.4
40-240	13.51	216.3	466.1	136.7
40-240 (SVD)	13.50	408.3	658.0	160.1